The Dynamics and Pinning of a Spike for a Reaction-Diffusion System

Michael J. Ward [1], Darragh McInerney [2], Paul Houston [3], David Gavaghan [4], Philip Maini [5].

Abstract

The motion of a one-spike solution to a simplified form of the Gierer-Meinhardt activator-inhibitor model is studied in both a one-dimensional and a two-dimensional domain. The pinning effect on the spike motion associated with the presence of spatially varying coefficients in the differential operator, referred to as precursor gradients, is studied in detail. In the one-dimensional case, we derive a differential equation for the trajectory of the spike in the limit $\varepsilon \to 0$, where ε is the activator diffusivity. A similar differential equation is derived for the two-dimensional problem in the limit for which $\varepsilon \ll 1$ and $D \gg 1$, where D is the inhibitor diffusivity. A numerical finite-element method is presented to track the motion of the spike for the full problem in both one and two dimensions. Finally, the numerical results for the spike motion are compared with corresponding asymptotic results for various examples.

1 Introduction

The generation of spatial pattern and form is one of the major unresolved problems in developmental biology. In 1952, Alan Turing [15] showed, mathematically, that a pair of reacting and diffusing chemicals could evolve from initial near spatially homogeneous states to spatially-varying states via the mechanism of local self-enhancement and long range inhibition. He hypothesized that the resultant chemical concentration profiles could serve as pre-patterns, providing information for cells, which would differentiate accordingly, forming a spatial pattern. He termed these chemicals "morphogens" and, although morphogens have yet to be uniequivocally identified in biological systems, Turing patterns in chemistry are now well-documented (for a review, see Maini *et al.* [11]).

Since Turing's seminal paper, a great number of reaction-diffusion models have been proposed for pattern formation. Perhaps the most well-known models are those of activator-inhibitor type postulated by Gierer and Meinhardt [6]. Their models not only generate spatial patterns, they also exhibit size regulation, a phenomenon that occurs in many developmental systems (they focussed on Hydra). They showed how reaction-diffusion models could markedly enhance pre-existing shallow spatial gradients, resulting in a highly localized (spike-type) pattern for the activator concentration.

[1]Department of Mathematics, University of British Columbia, Vancouver, Canada V6T 1Z2
[2]Mathematical Institute, Oxford University, Oxford, United Kingdom OX1 3LB
[3]Department of Mathematics and Computer Science, University of Leicester, University Road, Leicester, United Kingdom, LE1 7RH
[4]Computing Laboratory, Wolfson Building, Parks Road, Oxford University, Oxford, United Kingdom OX1 3QD
[5]Mathematical Institute, Oxford University, Oxford, United Kingdom OX1 3LB

Over the years there has been much numerical work classifying pattern formation aspects of this model, including the development of spikes and stripes (cf. [7], [12] and the references therein). A mathematical survey of results on spike solutions to the Gierer-Meinhardt model is given in [14].

The goal of this paper is to study the dynamics of localized solutions to a simplified form of the Gierer-Meinhardt (GM) model in a one-dimensional and a two-dimensional domain. The simplification to the GM model that is made is that we neglect the time dependence associated with the inhibitor field. With this simplification, in a one-dimensional domain the dimensionless GM model reduces to the following reaction-diffusion system of activator-inhibitor type (cf. [8]):

$$a_t = \varepsilon^2 a_{xx} - [1 + V(x)]\, a + \frac{a^p}{h^q}\,, \qquad -1 < x < 1\,, \quad t > 0\,, \tag{1.1a}$$

$$0 = D h_{xx} - \mu(x) h + \varepsilon^{-1} \frac{a^r}{h^s}\,, \qquad -1 < x < 1\,, \quad t > 0\,, \tag{1.1b}$$

$$a_x(\pm 1, t) = h_x(\pm 1, t) = 0\,. \tag{1.1c}$$

Here a, h, ε, $D > 0$, $\mu(x) > 0$, and $V = V(x) > 0$ represent the scaled activator concentration, inhibitor concentration, activator diffusivity, inhibitor diffusivity, inhibitor decay rate, and precursor gradient, respectively. The exponents (p, q, r, s) in (1.1) are assumed to satisfy

$$p > 1, \qquad q > 0, \qquad r > 0, \qquad s \geq 0, \qquad 0 < \frac{p-1}{q} < \frac{r}{s+1}\,. \tag{1.2}$$

Here we assume that $\varepsilon \ll 1$ so that the activator diffuses more slowly than does the inhibitor. The analogous problem in a two-dimensional domain is (cf. [8])

$$a_t = \varepsilon^2 \triangle a - [1 + V(\boldsymbol{x})]\, a + \frac{a^p}{h^q}\,, \qquad \boldsymbol{x} \in \Omega \quad t > 0\,, \tag{1.3a}$$

$$0 = D \triangle h - \mu(\boldsymbol{x}) h + \varepsilon^{-2} \frac{a^r}{h^s}\,, \qquad \boldsymbol{x} \in \Omega\,, \quad t > 0\,, \tag{1.3b}$$

$$\partial_n a = \partial_n h = 0\,, \qquad \boldsymbol{x} \in \partial\Omega\,. \tag{1.3c}$$

Here ∂_n is the outward normal derivative to the boundary and Ω is a bounded domain in $\mathcal{R}^2$. In the biological context, V and μ are examples of precursor gradients, and their biological significance is discussed in [7].

For $\varepsilon \ll 1$, many numerical studies of the GM model (1.1) (i. e. [6], [7]) have shown that the solution to (1.1) can have one or more spikes in the activator concentration a. These spikes, which represent strong localized deviations from a constant background concentration, have a spatial extent of $O(\varepsilon)$. In Fig. 1 we plot a one-spike equilibrium solution to (1.1) for $V \equiv 0$, $\mu \equiv 1$ and for certain other specific parameter values. In this case, an equilibrium one-spike solution is, by symmetry considerations, centered at the midpoint of the interval as shown in Fig. 1. However, the situation is very different when $V(x)$ and $\mu(x)$ are spatially varying. These terms can have many

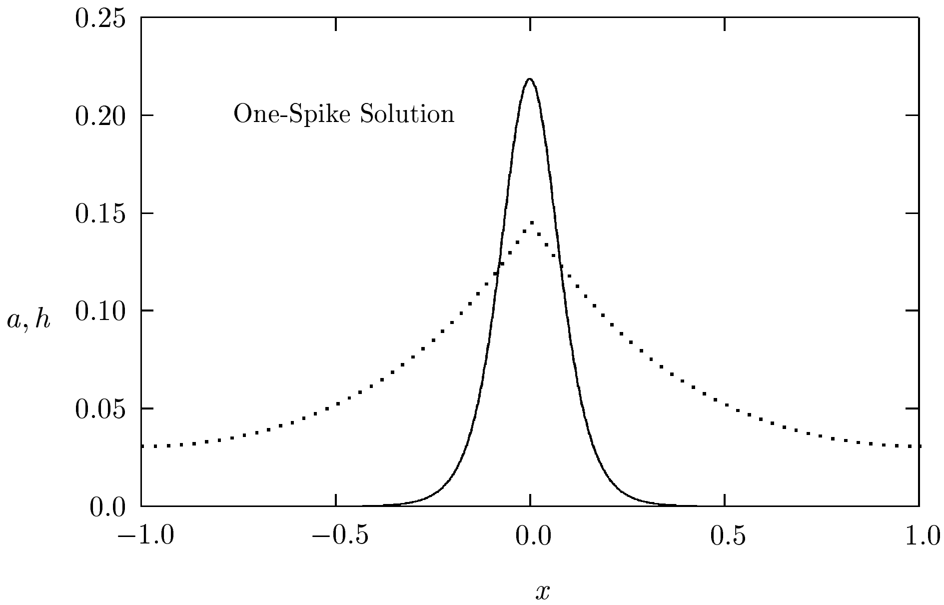

Figure 1: Plot of a one-spike equilibrium solution to (1.1) computed numerically with $(p, q, r, s) = (2, 1, 2, 0)$, $V \equiv 0$, $\epsilon = .05$, $\mu \equiv 1.0$ and $D = .20$. The solid curve is the activator concentration and the dotted curve is the inhibitor concentration.

interesting effects on the dynamics of spikes, on their equilibrium locations, and on the stability of equilibrium solutions. In particular, similar to the vortex dynamics problems in superconductivity studied in [3] and [10], we show that the motion of a spike can be pinned to certain points on the domain due to the presence of the precursor gradients.

The outline of the paper is as follows. In §2 we examine the effects of a spatially variable inhibitor decay rate $\mu = \mu(x) > 0$ and a potential $V(x)$ on the dynamics and the equilibrium locations of a one-spike solution to the one-dimensional problem (1.1). In particular, we derive an asymptotic differential equation for the center $x_0(t)$ of a one-spike solution to (1.1). We show that the exact equilibrium location now depends on certain pointwise values of $V(x)$ and on certain global properties associated with $\mu(x)$ over the domain. In §3 we treat the two-dimensional problem (1.3). In the interesting paper [5] a differential equation for the center of the spike was derived for the special case $p = 2$, $q = 1$, $V \equiv 0$ and $\mu \equiv 1$. We extend this result using the method of matched asymptotic expansions to derive a similar result for the more general case of arbitrary p and q, allowing V and μ to have a spatial dependence. The analysis is valid when $D \gg -\log \varepsilon$ and $\varepsilon \ll 1$. In §4 we present a finite element method to solve the one-dimensional and the two-dimensional problems (1.1) and (1.3) numerically. Finally, in §5 and §6 we compare the asymptotic results of §2 and §3 with corresponding numerical results obtained from the finite element method of §4 for the one-dimensional and the two-dimensional problems, respectively.

2 One-Spike Asymptotic Dynamics: The One-Dimensional Case

In this section we analyze the dynamics of a one-spike solution to (1.1). For finite inhibitor diffusivity D, we derive a differential equation determining the location $x_0(t)$ of the maximum of the activator concentration for a one-spike solution to (1.1).

In the inner region near the spike we introduce the new variables

$$y = \varepsilon^{-1}\left[x - x_0(\tau)\right], \qquad \tilde{h}(y) = h(x_0 + \varepsilon y), \qquad \tilde{a}(y) = a(x_0 + \varepsilon y), \qquad \tau = \varepsilon^2 t. \tag{2.1a}$$

We then expand the inner solution as

$$\tilde{h}(y) = \tilde{h}_0(y) + \varepsilon \tilde{h}_1(y) + \cdots, \qquad \tilde{a}(y) = \tilde{a}_0(y) + \varepsilon \tilde{a}_1(y) + \cdots. \tag{2.1b}$$

The spike location is chosen to satisfy $\tilde{a}'(0) = 0$. Substituting (2.1) into (1.1), and collecting terms that are $O(1)$ as $\varepsilon \to 0$, we obtain the leading order problems for $\tilde{a}_0$ and $\tilde{h}_0$

$$\tilde{a}_0'' - [1 + V(x_0)]\,\tilde{a}_0 + \tilde{a}_0^p/\tilde{h}_0^q = 0, \qquad -\infty < y < \infty, \tag{2.2a}$$

$$\tilde{h}_0'' = 0, \tag{2.2b}$$

with $\tilde{a}_0'(0) = 0$. In order to match to the outer solution to be constructed below we require that $\tilde{h}_0$ is independent of y. Thus, we set $\tilde{h}_0 = H$, where $H = H(\tau)$ is a function to be determined. We then write the solution to (2.2a) as

$$\tilde{a}_0(y) = H^\gamma u_c(y; x_0), \qquad \text{where} \qquad \gamma \equiv q/(p-1). \tag{2.2c}$$

Here $u_c(y)$ is the unique solution to

$$u_c'' - [1 + V(x_0)]\,u_c + u_c^p = 0, \qquad -\infty < y < \infty, \tag{2.3a}$$

$$u_c(0) > 0, \quad u_c'(0) = 0; \qquad u_c(y) \sim \alpha e^{-|y|}, \qquad \text{as} \quad y \to \pm\infty, \tag{2.3b}$$

for some $\alpha = \alpha(x_0) > 0$. In the special case for which $p = 2$, we can calculate explicitly that

$$u_c(y) = \frac{3}{2}[1 + V(x_0)]\,\mathrm{sech}^2\left(\sqrt{1 + V(x_0)}\,y/2\right). \tag{2.3c}$$

Next, we collect the $O(\varepsilon)$ terms in the inner region expansion. In this way, we obtain the problem for $\tilde{a}_1$ and $\tilde{h}_1$,

$$\tilde{a}_1'' - [1 + V(x_0)]\,\tilde{a}_1 + \frac{p\tilde{a}_0^{p-1}}{\tilde{h}_0^q}\tilde{a}_1 = \frac{q\tilde{a}_0^p}{\tilde{h}_0^{q+1}}\tilde{h}_1 - x_0'\tilde{a}_0' + yV'(x_0)\tilde{a}_0, \qquad -\infty < y < \infty, \tag{2.4a}$$

$$D\tilde{h}_1'' = -\tilde{a}_0^r/\tilde{h}_0^s. \tag{2.4b}$$

Here $x_0' \equiv dx_0/d\tau$. We then write $\tilde{a}_1$ as

$$\tilde{a}_1 = H^{\gamma} u_1 \,. \tag{2.5}$$

Substituting (2.2c), (2.5), and $\tilde{h}_0 \equiv H$ into (2.4), we get

$$L(u_1) \equiv u_1'' - [1 + V(x_0)]\, u_1 + p u_c^{p-1} u_1 = \frac{q u_c^p}{H} \tilde{h}_1 - x_0' u_c' + y V'(x_0) u_c \,, \qquad -\infty < y < \infty \,, \tag{2.6a}$$

$$D\tilde{h}_1'' = -H^{\gamma r - s} u_c^r \,, \tag{2.6b}$$

where u_1 is to decay exponentially as $|y| \to \infty$. Since $Lu_c' = 0$ and $u_c' \to 0$ exponentially as $|y| \to \infty$, the right-hand side of (2.6a) must satisfy the solvability condition that it is orthogonal to u_c'. From this condition, we obtain

$$\frac{q}{H} \int_{-\infty}^{\infty} u_c^p u_c' \tilde{h}_1 \, dy + V'(x_0) \int_{-\infty}^{\infty} y u_c u_c' \, dy = x_0' \int_{-\infty}^{\infty} \left(u_c'\right)^2 \, dy \,. \tag{2.7}$$

The second term on the left-hand side of (2.7) is evaluated as

$$V'(x_0) \int_{-\infty}^{\infty} y u_c u_c' \, dy = -\frac{V'(x_0)}{2} \int_{-\infty}^{\infty} u_c^2 \, dy \,. \tag{2.8}$$

To evaluate the first term on the left-hand side of (2.7) we integrate by parts twice, and use the facts that $\tilde{h}_1''$ and u_c are even functions. In this way, we get the differential equation

$$x_0' \int_{-\infty}^{\infty} \left(u_c'\right)^2 \, dy = -\frac{q}{2H(p+1)} \int_{-\infty}^{\infty} u_c^{p+1} \, dy \left(\lim_{y \to +\infty} \tilde{h}_1' + \lim_{y \to -\infty} \tilde{h}_1' \right) - \frac{V'(x_0)}{2} \int_{-\infty}^{\infty} u_c^2 \, dy \,. \tag{2.9}$$

Next, we analyze the solution in the outer region defined at an $O(1)$ distance away from the center of the spike. In this region, a is exponentially small and we expand h as $h = h_0(x) + o(1)$ as $\varepsilon \to 0$. Then, from (1.1b), we obtain that h_0 satisfies

$$Dh_0'' - \mu h_0 = -H^{\gamma r - s} b_r \delta(x - x_0) \,, \qquad -1 < x < 1 \,, \tag{2.10a}$$

$$h_0'(\pm 1) = 0 \,. \tag{2.10b}$$

Here $b_r = b_r(x_0)$ is defined by

$$b_r \equiv \int_{-\infty}^{\infty} \left[u_c(y)\right]^r \, dy \,. \tag{2.10c}$$

Solving for h_0 we have

$$h_0(x) = H^{\gamma r - s} b_r G(x; x_0) \,, \tag{2.11}$$

where the Green's function $G(x;x_0)$ satisfies

$$DG_{xx} - \mu G = -\delta(x - x_0)\,, \qquad -1 < x < 1\,, \tag{2.12a}$$

$$G_x(\pm 1; x_0) = 0\,. \tag{2.12b}$$

To match the outer and inner solutions we require that

$$h_0(x_0) = H\,, \qquad \lim_{y\to+\infty} \tilde{h}_1' + \lim_{y\to-\infty} \tilde{h}_1' = h_0'(x_{0+}) + h_0'(x_{0-})\,. \tag{2.13}$$

Substituting (2.11) into (2.13), we get

$$\lim_{y\to+\infty} \tilde{h}_1' + \lim_{y\to-\infty} \tilde{h}_1' = \frac{H}{G(x_0;x_0)} \left[G_x(x_{0+};x_0) + G_x(x_{0-};x_0)\right]\,, \tag{2.14a}$$

$$H = \left[\frac{1}{b_r G(x_0;x_0)}\right]^{1/[\gamma r - (s+1)]}\,. \tag{2.14b}$$

Finally, substituting (2.14) into (2.2c), (2.9) and (2.11), and letting $\tau = \varepsilon^2 t$, we obtain the main result of this section:

Proposition 2.1: *For $\varepsilon \ll 1$, the dynamics of a one-spike solution to (1.1) is characterized by*

$$a(x,t) \sim H^{\gamma} u_c\left(\varepsilon^{-1}[x - x_0(t)]; x_0\right)\,, \tag{2.15a}$$

$$h(x,t) \sim HG\left[x; x_0(t)\right] / G\left[x_0(t); x_0(t)\right]\,, \tag{2.15b}$$

where $H = H(t)$ is given in (2.14b). The spike location $x_0(t)$ satisfies the differential equation

$$\frac{dx_0}{dt} \int_{-\infty}^{\infty} \left[u_c'(y)\right]^2 \, dy \sim -\frac{\varepsilon^2 q}{2(p+1)} \int_{-\infty}^{\infty} [u_c(y)]^{p+1} \, dy \left(\frac{G_x(x_{0+};x_0) + G_x(x_{0-};x_0)}{G(x_0;x_0)}\right) - \frac{\varepsilon^2}{2} V'(x_0) \int_{-\infty}^{\infty} [u_c(y)]^2 \, dy\,. \tag{2.15c}$$

Notice that when $V(x_0) \neq 0$, the integrals in (2.15c) may also depend on x_0.

We can calculate the integrals in (2.15c) explicitly using the differential equation (2.3) for u_c. As shown in Appendix A, we get

$$\frac{\int_{-\infty}^{\infty} [u_c(y)]^{p+1} \, dy}{\int_{-\infty}^{\infty} [u_c'(y)]^2 \, dy} = \frac{2(p+1)}{p-1}\,; \qquad \frac{\int_{-\infty}^{\infty} [u_c(y)]^2 \, dy}{\int_{-\infty}^{\infty} [u_c'(y)]^2 \, dy} = \left(\frac{p+3}{p-1}\right) \left[1 + V(x_0)\right]^{-1}\,. \tag{2.16}$$

Substituting (2.16) into (2.15c) we obtain the following result:

Corollary 2.1: *For $\varepsilon \ll 1$, the dynamics of a one-spike solution to (1.1) is characterized by*

$$\frac{dx_0}{dt} \sim -\frac{\varepsilon^2 q}{p-1} \left(\frac{G_x(x_{0+};x_0) + G_x(x_{0-};x_0)}{G(x_0;x_0)}\right) - \frac{\varepsilon^2}{2} \left(\frac{p+3}{p-1}\right) \frac{V'(x_0)}{1 + V(x_0)}\,. \tag{2.17}$$

We now study the effect of $\mu(x)$ on the dynamics.

2.1 The effect of $\mu(x)$

In the special case where $\mu(x) = \mu$ is a positive constant independent of x, we can solve (2.12) explicitly for $G(x;x_0)$ to get

$$G(x;x_0) = \begin{cases} A_0 \cosh\left[\theta(1+x)\right] / \cosh\left[\theta(1+x_0)\right], & -1 < x < x_0\,, \\ A_0 \cosh\left[\theta(1-x)\right] / \cosh\left[\theta(1-x_0)\right], & x_0 < x < 1\,, \end{cases} \tag{2.18a}$$

where

$$A_0 \equiv \frac{1}{\sqrt{\mu D}} \left(\tanh\left[\theta(1-x_0)\right] + \tanh\left[\theta(1+x_0)\right]\right)^{-1}\,, \qquad \theta \equiv (\mu/D)^{1/2}\,. \tag{2.18b}$$

Substituting (2.18) into (2.17), we obtain the following result:
Corollary 2.2: *Let $\varepsilon \ll 1$ and $\mu(x) = \mu$ be a positive constant. Then, the differential equation for the spike location is*

$$\frac{dx_0}{dt} \sim -\frac{\varepsilon^2 q\theta}{p-1} \left(\tanh\left[\theta(1+x_0)\right] - \tanh\left[\theta(1-x_0)\right]\right) - \frac{\varepsilon^2}{2} \left(\frac{p+3}{p-1}\right) \frac{V'(x_0)}{1+V(x_0)}\,. \tag{2.19}$$

Here $\theta \equiv \sqrt{\mu/D}$.

From (2.19) we can see the qualitative effect of the potential term $V(x)$ on the stability of a one-spike solution. If V is convex with a minimum at some point in $[-1,1]$ then there exists a unique equilibrium solution to (2.19). The situation is more complicated when $V(x)$ is not convex. For instance, suppose that $V(x)$ is a double-well potential of the form $V(x) = \zeta(1-x^2)^2$ with $\zeta > 0$. Then, it is easy to see from (2.19) that when $\zeta > q\theta^2 \text{sech}^2\theta/[p+3]$, $x_0 = 0$ is an unstable equilibrium solution to (2.19) and there exists a stable equilibrium solution on each of the subintervals $-1 < x < 0$ and $0 < x < 1$.

In general, when μ depends on x we must compute the Green's function satisfying (2.12) to determine the dynamics as described in (2.17). However, to illustrate qualitatively the effect of a spatially varying $\mu(x)$, we now derive an approximate differential equation for x_0 in the limits $D \gg 1$ and $D \ll 1$, with D independent of ε.

In the limit $D \gg 1$, we expand G as

$$G(x;x_0) = G_0(x;x_0) + D^{-1} G_1(x;x_0) + O\left(D^{-2}\right)\,. \tag{2.20}$$

Substituting (2.20) into (2.12), and collecting powers of D^{-1}, we get

$$G_{0xx} = 0\,; \qquad G_{1xx} = \mu G_0 - \delta(x - x_0)\,, \tag{2.21}$$

with $G_{jxx} = 0$ at $x = \pm 1$ for $j = 0,1$. The problem for G_1 does not have a solution unless G_0 satisfies a solvability condition. In this way, we calculate that

$$G_0 = (2\mu_a)^{-1}\,; \qquad G_{1x} = (2\mu_a)^{-1} \int_{-1}^{x} \mu(y)\, dy - \begin{cases} 0 & -1 < x < x_0\,, \\ 1 & x_0 < x < 1\,. \end{cases} \tag{2.22}$$

Here μ_a is the average of μ over the interval, defined by

$$\mu_a \equiv \frac{1}{2} \int_{-1}^{1} \mu(x)\, dx \,. \tag{2.23}$$

Substituting (2.22) into (2.19) we obtain the following result:

Corollary 2.3: *For $\varepsilon \ll 1$ and $D \gg 1$, with D independent of ε, the differential equation (2.17) for the spike location reduces to*

$$\frac{dx_0}{dt} \sim -\frac{2\varepsilon^2 q}{D(p-1)} \left(\int_{-1}^{x_0} \mu(y)\, dy - \mu_a \right) - \frac{\varepsilon^2}{2} \left(\frac{p+3}{p-1} \right) \frac{V'(x_0)}{1+V(x_0)} \,. \tag{2.24}$$

Alternatively, when $D \ll 1$, we can readily obtain a WKB solution for (2.12) in the form

$$G(x;x_0) = \begin{cases} A_0 \mu^{-1/2} \cosh \left[D^{-1/2} \int_{-1}^{x} \sqrt{\mu(s)}\, ds \right] / \cosh \left[D^{-1/2} \int_{-1}^{x_0} \sqrt{\mu(s)}\, ds \right], & -1 < x < x_0 \,, \\ A_0 \mu^{-1/4} \cosh \left[D^{-1/2} \int_{x}^{1} \sqrt{\mu(s)}\, ds \right] / \cosh \left[D^{-1/2} \int_{x_0}^{1} \sqrt{\mu(s)}\, ds \right], & x_0 < x < 1 \,, \end{cases} \tag{2.25a}$$

where

$$A_0 \equiv \frac{1}{\sqrt{D}\mu^{1/4}} \left(\tanh \left[D^{-1/2} \int_{x_0}^{1} \sqrt{\mu(s)}\, ds \right] + \tanh \left[D^{-1/2} \int_{-1}^{x_0} \sqrt{\mu(s)}\, ds \right] \right)^{-1} \,. \tag{2.25b}$$

Substituting (2.25) into (2.19), we obtain the next result.

Corollary 2.4: *For $\varepsilon \ll 1$ and $D \ll 1$, with D independent of ε, the differential equation (2.17) for the spike location reduces to*

$$\begin{aligned} \frac{dx_0}{dt} \sim -\frac{\varepsilon^2 q}{p-1} \sqrt{\frac{\mu}{D}} \left[\tanh \left(D^{-1/2} \int_{-1}^{x_0} \sqrt{\mu(s)}\, ds \right) - \tanh \left(D^{-1/2} \int_{x_0}^{1} \sqrt{\mu(s)}\, ds \right) \right] \\ - \frac{\varepsilon^2}{2} \left(\frac{p+3}{p-1} \right) \frac{V'(x_0)}{1+V(x_0)} \,. \end{aligned} \tag{2.26}$$

From (2.24) and (2.26) we observe that the one-spike dynamics depends on global properties associated with $\mu(x)$ but on pointwise properties associated with $V(x)$.

3 One-Spike Asymptotic Dynamics: The Two-Dimensional Case

In this section we analyze the dynamics of a one-spike solution to (1.3) in the limit $\varepsilon \ll 1$ and $D \gg 1$. Our goal is to derive a differential equation for the center $\boldsymbol{x_0}$ of the spike as a function of time. In the limit $\varepsilon \ll 1$ and $D \gg 1$, the solution in the inner region, referred to as the core of the spike, has the leading order asymptotic form

$$a(\boldsymbol{x},t) \sim a_0(|\boldsymbol{y}|) \equiv \mathcal{H}^\gamma u_c(|\boldsymbol{y}|)\,, \tag{3.1a}$$
$$h(\boldsymbol{x},t) \sim \mathcal{H}\,. \tag{3.1b}$$

Here $\gamma = q/(p-1)$, $\boldsymbol{y} = \varepsilon^{-1}(\boldsymbol{x}-\boldsymbol{x_0})$ and $\mathcal{H}$ is some constant to be determined. The radially symmetric function $u_c(|\boldsymbol{y}|)$, with $\rho = |\boldsymbol{y}|$, is the unique positive solution of

$$u_c^{''} + \frac{1}{\rho}u_c^{'} - [1+V(\boldsymbol{x_0})]\,u_c + u_c^p = 0\,, \qquad \rho \geq 0\,, \tag{3.2a}$$
$$u_c^{'}(0) = 0\,; \qquad u_c \sim \alpha\rho^{-1/2}e^{-\beta\rho}\,, \quad \text{as} \quad \rho \to \infty\,. \tag{3.2b}$$

Here $\alpha = \alpha(\boldsymbol{x_0}) > 0$ is some constant and $\beta = \sqrt{1+V(\boldsymbol{x_0})}$. The function u_c depends on $\boldsymbol{x_0}$, so that the activator concentration in the core depends on the location of the spike.

In the outer region, away from the core of the spike, a is exponentially small and so the term $\varepsilon^{-2}a^r/h^s$ in (1.3b) will be exponentially small except when $\boldsymbol{x}$ approaches $\boldsymbol{x_0}$. In the outer region, this term is asymptotically represented as a multiple of a Dirac mass in the form

$$\varepsilon^{-2}\frac{a^r}{h^s} \to 2\pi\mathcal{H}^{\gamma r - s}b_r\delta(\boldsymbol{x}-\boldsymbol{x_0})\,, \qquad b_r \equiv \int_0^\infty [u_c(\rho)]^r\,\rho\,d\rho\,, \tag{3.3}$$

where $u_c(\rho)$ satisfies (3.2). Substituting (3.3) into (1.3b), we see that the outer problem for h is

$$D\triangle h - \mu h + 2\pi\mathcal{H}^{\gamma r - s}b_r\delta(\boldsymbol{x}-\boldsymbol{x_0}) = 0\,, \qquad \boldsymbol{x} \in \Omega\,, \tag{3.4a}$$
$$\partial_n h = 0\,, \qquad \boldsymbol{x} \in \partial\Omega\,. \tag{3.4b}$$

We now solve this problem for $D \gg 1$ by expanding h as

$$h = h_0 + \frac{1}{D}h_1 + \frac{1}{D^2}h_2 + \cdots\,. \tag{3.5}$$

Substituting (3.5) into (3.4), and collecting powers of D^{-1}, we obtain

$$\triangle h_0 = 0\,, \qquad \boldsymbol{x} \in \Omega\,; \qquad \partial_n h_0 = 0\,, \qquad \boldsymbol{x} \in \partial\Omega\,, \tag{3.6}$$

and

$$\triangle h_1 = \mu h_0 - 2\pi\mathcal{H}^{\gamma r - s}b_r\delta(\boldsymbol{x}-\boldsymbol{x_0})\,, \qquad \boldsymbol{x} \in \Omega\,, \tag{3.7a}$$
$$\partial_n h_1 = 0\,, \qquad \boldsymbol{x} \in \partial\Omega\,, \tag{3.7b}$$
$$\int_\Omega \mu h_1\,d\boldsymbol{x} = 0\,. \tag{3.7c}$$

This last condition, which arises from a solvability condition applied to the problem for h_2, ensures that the solution to (3.7) is unique.

The solution to (3.6) depends only on time. To match this solution to the inner solution we require

$$h_0 = \mathcal{H} . \tag{3.8}$$

The divergence theorem applied to (3.7) determines $\mathcal{H}$ as

$$\mathcal{H} = \left(\frac{2\pi b_r}{\int_\Omega \mu \, d\boldsymbol{x}} \right)^{\frac{1}{(1+s)-\gamma r}} . \tag{3.9}$$

Then, with this value of $\mathcal{H}$, we write the solution to (3.7) as

$$h_1 = \mathcal{H} G(\boldsymbol{x}; \boldsymbol{x_0}) \int_\Omega \mu \, d\boldsymbol{x} , \tag{3.10}$$

where G is the modified Green's function satisfying

$$\triangle G = \frac{\mu}{\int_\Omega \mu \, d\boldsymbol{x}} - \delta(\boldsymbol{x} - \boldsymbol{x_0}) , \qquad \boldsymbol{x} \in \Omega , \tag{3.11a}$$

$$\partial_n G = 0 , \qquad \boldsymbol{x} \in \partial\Omega , \tag{3.11b}$$

$$\int_\Omega \mu G \, d\boldsymbol{x} = 0 . \tag{3.11c}$$

The two-term expansion obtained from substituting (3.8) and (3.10) into (3.5) is

$$h \sim \mathcal{H} \left(1 + \frac{G(\boldsymbol{x}; \boldsymbol{x_0})}{D} \int_\Omega \mu \, d\boldsymbol{x} \right) . \tag{3.12}$$

The solution to (3.11) can be written as a sum of a singular part and a regular part R as

$$G(\boldsymbol{x}; \boldsymbol{x_0}) = -\frac{1}{2\pi} \log |\boldsymbol{x} - \boldsymbol{x_0}| + R(\boldsymbol{x}; \boldsymbol{x_0}) . \tag{3.13}$$

As $\boldsymbol{x} \to \boldsymbol{x_0}$ we can expand R in a Taylor series as

$$R(\boldsymbol{x}; \boldsymbol{x_0}) = R_0 + \boldsymbol{\nabla} R_0 \cdot (\boldsymbol{x} - \boldsymbol{x_0}) + \cdots , \qquad R_0 \equiv R(\boldsymbol{x_0}; \boldsymbol{x_0}) , \quad \boldsymbol{\nabla} R_0 \equiv \boldsymbol{\nabla} R(\boldsymbol{x}; \boldsymbol{x_0})|_{\boldsymbol{x}=\boldsymbol{x_0}} . \tag{3.14}$$

Therefore, the two-term expansion (3.12) for h has the following behavior as $\boldsymbol{x} \to \boldsymbol{x_0}$:

$$h \sim \mathcal{H} \left[1 + \frac{1}{D} \int_\Omega \mu \, d\boldsymbol{x} \left(-\frac{1}{2\pi} \log |\boldsymbol{x} - \boldsymbol{x_0}| + R_0 + \boldsymbol{\nabla} R_0 \cdot (\boldsymbol{x} - \boldsymbol{x_0}) \right) \right] . \tag{3.15}$$

We now construct the inner expansion and derive the differential equation for $\boldsymbol{x_0}$ in two limiting regimes of D and ε.

3.1 The Effect of the Potential

The form (3.15) suggests that in the inner (core) region the change in h from a constant value will be of the order $O(-\log\varepsilon/D)$. In this region, the perturbation to a induced by the gradient of the potential is of the order $O(\varepsilon)$. Hence, as $\varepsilon \to 0$, we will assume at present that D is large enough to satisfy

$$D \gg -\varepsilon^{-1}\log\varepsilon\,. \tag{3.16}$$

This restriction on D can be weakened substantially as discussed following (3.38) below. Under (3.16) we can expand a and h in the core region as

$$a(\boldsymbol{x},t) = \mathcal{H}^{\gamma}u_c\left[\varepsilon^{-1}(\boldsymbol{x}-\boldsymbol{x_0}(\tau))\right] + \varepsilon\tilde{a}_1 + \cdots\,, \qquad h = \mathcal{H} + o(\varepsilon)\,, \tag{3.17}$$

where $\tau = \varepsilon^2 t$. Substituting (3.17) into (1.3a), and writing $\tilde{a}_1$ as

$$\tilde{a}_1 = \mathcal{H}^{\gamma}u_1\,, \tag{3.18}$$

we get that u_1 satisfies

$$L(u_1) \equiv \triangle u_1 - \left[1+V(\boldsymbol{x_0})\right]u_1 + pu_c^{p-1}u_1 = \boldsymbol{\nabla}V(\boldsymbol{x_0})\cdot\boldsymbol{y}\,u_c - u_c^{'}\frac{\boldsymbol{x_0}^{'}\cdot\boldsymbol{y}}{|\boldsymbol{y}|}\,. \tag{3.19}$$

Here $\boldsymbol{x_0}^{'} \equiv d\boldsymbol{x_0}/d\tau$ and $u_1 \to 0$ is to tend exponentially to zero as $|\boldsymbol{y}| \to \infty$. Since $L\left(\partial_{y_j}u_c\right) = 0$ for $j = 1,2$, this problem for u_1 has a solution only when the right-hand side of (3.19) is orthogonal to $\partial_{y_j}u_c$ for $j = 1,2$. Hence, the solvability condition for (3.19) is

$$\boldsymbol{x_0}^{'}\cdot\int_{\mathcal{R}^2}\frac{\boldsymbol{y}}{|\boldsymbol{y}|}u_c^{'}\partial_{y_j}u_c\,d\boldsymbol{y} = \boldsymbol{\nabla}V(\boldsymbol{x_0})\cdot\int_{\mathcal{R}^2}\boldsymbol{y}\,u_c\partial_{y_j}u_c\,d\boldsymbol{y}\,, \tag{3.20}$$

for $j = 1,2$. Upon integrating by parts and using symmetry we can readily derive that

$$\int_{\mathcal{R}^2} y_k u_c\partial_{y_j}u_c\,d\boldsymbol{y} = -\pi\int_0^{\infty}\left[u_c(\rho)\right]^2\rho\,d\rho\,\delta_{j,k}\,; \qquad \int_{\mathcal{R}^2}\frac{y_k}{|\boldsymbol{y}|}u_c^{'}\partial_{y_j}u_c\,d\boldsymbol{y} = \pi\int_0^{\infty}\left[u_c^{'}(\rho)\right]^2\rho\,d\rho\,\delta_{j,k}\,. \tag{3.21}$$

Here $\delta_{j,k}$ is the usual Kronecker symbol. Substituting (3.21) into (3.20) we obtain the following main result:

Proposition 3.1: *For $\varepsilon \ll 1$ and D satisfying (3.16), the dynamics of a one-spike solution to (1.3) in the core is characterized by*

$$a(x,t) \sim \mathcal{H}u_c\left[\varepsilon^{-1}|\boldsymbol{x}-\boldsymbol{x_0}(t)|\right] + O(\varepsilon)\,, \tag{3.22a}$$

$$h(x,t) \sim \mathcal{H} + o(\varepsilon)\,, \tag{3.22b}$$

where u_c and $\mathcal{H}$ are defined in (3.2) and (3.9), respectively. The differential equation for the center $\boldsymbol{x_0}$ of the spike is

$$\frac{d\boldsymbol{x_0}}{dt} \sim -\varepsilon^2 \boldsymbol{\nabla} V(\boldsymbol{x_0}) \left(\frac{\int_0^\infty [u_c(\rho)]^2 \rho \, d\rho}{\int_0^\infty [u_c'(\rho)]^2 \rho \, d\rho} \right) . \tag{3.22c}$$

Notice that since u_c depends on $\boldsymbol{x_0}$ as seen from (3.2), the integrals in (3.22c) may also depend on $\boldsymbol{x_0}$. To explicitly show this dependence, we introduce the new variables η and w_c defined by

$$\rho = [1 + V(\boldsymbol{x_0})]^{-1/2} \eta \,, \qquad u_c = [1 + V(\boldsymbol{x_0})]^{1/(p+1)} w_c \,. \tag{3.23}$$

Substituting (3.23) into (3.2), we find that $w_c(\eta)$ satisfies

$$w_c'' + \frac{1}{\eta} w_c' - w_c + w_c^p = 0 \,, \qquad \eta \geq 0 \,, \tag{3.24a}$$

$$w_c'(0) = 0 \,; \qquad w_c \sim \alpha \eta^{-1/2} e^{-\eta} \,, \quad \text{as} \quad \eta \to \infty \,. \tag{3.24b}$$

In terms of these variables (3.22c) becomes

$$\frac{d\boldsymbol{x_0}}{dt} \sim -\varepsilon^2 b \frac{\boldsymbol{\nabla} V(\boldsymbol{x_0})}{1 + V(\boldsymbol{x_0})} \,, \qquad b \equiv \frac{\int_0^\infty [w_c(\eta)]^2 \eta \, d\eta}{\int_0^\infty [w_c'(\eta)]^2 \eta \, d\eta} \,, \tag{3.25}$$

where b is independent of $\boldsymbol{x_0}$. In Appendix B we calculate b as $b = 2/(p-1)$. Then, (3.22c) can be written compactly as the gradient flow

$$\frac{d\boldsymbol{x_0}}{dt} \sim -\frac{2\varepsilon^2}{(p-1)} \boldsymbol{\nabla} W(\boldsymbol{x_0}) \,, \qquad \text{where} \qquad W(\boldsymbol{x_0}) \equiv \log\left[1 + V(\boldsymbol{x_0})\right] \,. \tag{3.26}$$

From (3.26) we observe that stable equilibria for the spike are located at points where the potential $V(\boldsymbol{x})$ has a local minimum. In addition, the motion of the spike is orthogonal to level curves of the potential $W(\boldsymbol{x_0})$ and $dW(\boldsymbol{x_0})/dt < 0$ except at critical points of W.

3.2 The Regular Part of the Green's function

In the derivation below we assume that $V(\boldsymbol{x}) \equiv 0$ in (1.3). Our expansion parameter is taken as ε/D and we will use $D \gg 1$ to simplify some of the terms that arise in the expansion. In the core region we begin by introducing new variables by

$$\tilde{a}(\boldsymbol{y}) = a(\boldsymbol{x_0} + \varepsilon \boldsymbol{y}, t) \,, \qquad \tilde{h}(\boldsymbol{y}) = h(\boldsymbol{x_0} + \varepsilon \boldsymbol{y}, t) \,, \qquad \boldsymbol{y} = \varepsilon^{-1} \left[\boldsymbol{x} - \boldsymbol{x_0}(\tau)\right] \,, \tag{3.27}$$

where τ is a slow time scale. We then expand $\tilde{a}$ and $\tilde{h}$ as

$$\tilde{a}(\boldsymbol{y}) = \tilde{a}_0(|\boldsymbol{y}|) + \frac{\varepsilon}{D} \tilde{a}_1(\boldsymbol{y}) + \cdots \,, \qquad \tilde{h}(\boldsymbol{y}) = \tilde{h}_0(|\boldsymbol{y}|) + \frac{\varepsilon}{D} \tilde{h}_1(\boldsymbol{y}) + \cdots \,. \tag{3.28}$$

Here $\tilde{a}_0$ and $\tilde{h}_0$ are radially symmetric and are at most $O(-\log\varepsilon)$ as $\varepsilon \to 0$. The functions $\tilde{a}_1$ and $\tilde{h}_1$ are not radially symmetric. A nontrivial solvability condition will arise at the problem for $\tilde{a}_1$ and $\tilde{h}_1$. This forces us to introduce the slow time scale τ defined by

$$\tau = \frac{\varepsilon^2}{D} t\,. \tag{3.29}$$

Substituting (3.28) and (3.29) into (1.3a) and (1.3b), and collecting powers of ε/D, we obtain the problems

$$\triangle \tilde{a}_0 - \tilde{a}_0 + \frac{\tilde{a}_0^p}{\tilde{h}_0^q} = 0\,, \qquad |\boldsymbol{y}| \geq 0\,, \tag{3.30a}$$

$$\triangle \tilde{h}_0 = -\frac{\tilde{a}_0^r}{D\tilde{h}_0^s}\,, \qquad |\boldsymbol{y}| \geq 0\,, \tag{3.30b}$$

and

$$\triangle \tilde{a}_1 - \tilde{a}_1 + \frac{p\tilde{a}_0^{p-1}}{\tilde{h}_0^q}\tilde{a}_1 = \frac{q\tilde{a}_0^p}{\tilde{h}_0^{q+1}}\tilde{h}_1 - \tilde{a}_0' \frac{\boldsymbol{x_0}' \cdot \boldsymbol{y}}{|\boldsymbol{y}|}\,, \qquad \boldsymbol{y} \in \mathcal{R}^2\,, \tag{3.31a}$$

$$\triangle \tilde{h}_1 = -\frac{1}{D}\left[\frac{r\tilde{a}_0^{r-1}}{\tilde{h}_0^s}\tilde{a}_1 - \frac{s\tilde{a}_0^r}{\tilde{h}_0^{s+1}}\tilde{h}_1\right]\,, \qquad \boldsymbol{y} \in \mathcal{R}^2\,. \tag{3.31b}$$

Here $\boldsymbol{x_0}' \equiv d\boldsymbol{x_0}/d\tau$. The matching conditions as $|\boldsymbol{y}| \to \infty$ obtained from (3.15) are

$$\tilde{h}_0 \sim \mathcal{H}\left[1 + \frac{1}{D}\int_\Omega \mu\, d\boldsymbol{x}\left(-\frac{1}{2\pi}\log|\boldsymbol{y}| + \frac{1}{2\pi}\log\varepsilon + R_0\right)\right]\,, \qquad \text{as} \quad |\boldsymbol{y}| \to \infty\,, \tag{3.32a}$$

$$\tilde{h}_1 \sim \mathcal{H}\int_\Omega \mu\, d\boldsymbol{x}\ (\boldsymbol{\nabla} R_0 \cdot \boldsymbol{y}) \qquad \text{as} \quad |\boldsymbol{y}| \to \infty\,. \tag{3.32b}$$

When $D \gg 1$, there is a unique solution to (3.30) that has the following leading order expansion in D:

$$\tilde{a}_0 = \mathcal{H}^\gamma w_c(|\boldsymbol{y}|) + O(D^{-1})\,; \qquad \tilde{h}_0 \sim \mathcal{H} + O(D^{-1})\,. \tag{3.33}$$

Here $\mathcal{H}$ and w_c were defined in (3.9) and (3.24), respectively. In the limit $D \gg 1$, the solvability condition for (3.31a) is that the right-hand side of (3.31a) must be orthogonal to $\partial_{y_j} w_c$ for $j = 1, 2$. This condition yields a differential equation for $\boldsymbol{x_0}$ in the form

$$\boldsymbol{x_0}' \cdot \int_{\mathcal{R}^2} \frac{\boldsymbol{y}}{|\boldsymbol{y}|}\tilde{a}_0' \partial_{y_j} w_c\, d\boldsymbol{y} = \int_{\mathcal{R}^2} \frac{q\tilde{a}_0^p}{\tilde{h}_0^{q+1}}\tilde{h}_1\, \partial_{y_j} w_c\, d\boldsymbol{y}\,. \tag{3.34}$$

To derive an explicit differential equation, we substitute (3.33) into (3.34) to get

$$\boldsymbol{x_0}' \cdot \int_{\mathcal{R}^2} \frac{\boldsymbol{y}}{|\boldsymbol{y}|} w_c' \partial_{y_j} w_c \, d\boldsymbol{y} = \frac{q}{(p+1)\mathcal{H}} \int_{\mathcal{R}^2} \tilde{h}_1 \partial_{y_j} \left(w_c^{p+1} \right) \, d\boldsymbol{y} \,, \qquad j = 1, 2 \,. \tag{3.35}$$

The integral term on the left-hand side of (3.35) was evaluated in (3.21). To evaluate the integral term on the right-hand side of (3.35) we integrate by parts twice and use both symmetry and the asymptotic boundary condition (3.32b) as $\boldsymbol{y} \to \infty$ to get

$$\int_{\mathcal{R}^2} \tilde{h}_1 \boldsymbol{\nabla} \left(w_c^{p+1} \right) \, d\boldsymbol{y} = - \int_{\mathcal{R}^2} \left(w_c^{p+1} \right) \boldsymbol{\nabla} \tilde{h}_1 \, d\boldsymbol{y} \sim -\mathcal{H} \, \boldsymbol{\nabla} R_0 \int_{\Omega} \mu \, d\boldsymbol{x} \int_{\mathcal{R}^2} w_c^{p+1} \, d\boldsymbol{y} \,. \tag{3.36}$$

Substituting (3.36) and (3.21) into (3.35), we obtain the following result:

Proposition 3.2: *Consider a one-spike solution to (1.3) when $V(\boldsymbol{x}) = 0$, $\varepsilon \ll 1$ and $D \gg 1$. Then, the solution to (1.3) in the core is given by (3.22a) and (3.22b). The motion of the center of the spike satisfies*

$$\frac{d\boldsymbol{x_0}}{dt} \sim - \frac{2q\varepsilon^2}{D(p+1)} \boldsymbol{\nabla} R_0 \int_{\Omega} \mu \, d\boldsymbol{x} \left(\frac{\int_0^\infty \left[w_c(\rho) \right]^{p+1} \rho \, d\rho}{\int_0^\infty \left[w_c'(\rho) \right]^2 \rho \, d\rho} \right) . \tag{3.37}$$

Here $\boldsymbol{\nabla} R_0$ is the gradient of the regular part of the Green's function defined in (3.14). Setting $\mu = 1$, $p = 2$ and $q = 1$ in (3.37), we obtain the result derived previously in [5] using a different method.

As shown in Appendix B we can calculate the integral appearing in (3.37) exactly as

$$\frac{\int_0^\infty \left[w_c(\rho) \right]^{p+1} \rho \, d\rho}{\int_0^\infty \left[w_c'(\rho) \right]^2 \rho \, d\rho} = \frac{p+1}{p-1} \,. \tag{3.38}$$

There are two important remarks. The first observation is that the differential equation (3.37) derived when $V(\boldsymbol{x}) \equiv 0$ predicts a motion on a time scale of $O\left(\varepsilon^2/D\right)$ whereas (3.22c) predicts a motion on a faster time scale of $O(\varepsilon^2)$. Therefore, when $D \gg 1$, the pinning effect induced by the potential dominates the dynamics. The second observation concerns the range of validity of the results (3.22c) and (3.37) with respect to D. The key condition that allows for the analysis leading to (3.37) to be valid is that the problem (3.30) for $\tilde{a}_0$ and $\tilde{h}_0$ becomes uncoupled when $D \gg 1$. This ensures that $\tilde{h}_0 \sim \mathcal{H} + o(1)$ in the core region. By examining the asymptotic boundary condition for $\tilde{h}_0$ in (3.32a) we see that this condition holds when $D \gg -\log \varepsilon$. The same reasoning pertains to the derivation of (3.22c). Hence both (3.22c) and (3.37) are valid when $D \gg -\log \varepsilon$.

3.3 Calculating the Regular Part of the Green's Function

We decompose the solution to (3.11) in the form

$$G(\boldsymbol{x}; \boldsymbol{x_0}) = g_p(\boldsymbol{x}) + g(\boldsymbol{x}; \boldsymbol{x_0}) + c(\boldsymbol{x_0}) \,. \tag{3.39}$$

Here g_p and g are any solutions to

$$\triangle g_p = \frac{\mu}{\int_\Omega \mu \, d\boldsymbol{x}} \,, \qquad \boldsymbol{x} \in \Omega \,, \tag{3.40a}$$

$$\partial_n g_p = 1/L \,, \qquad \boldsymbol{x} \in \partial\Omega \,, \tag{3.40b}$$

and

$$\triangle g = -\delta(\boldsymbol{x} - \boldsymbol{x_0}) \,, \qquad \boldsymbol{x} \in \Omega \,, \tag{3.41a}$$

$$\partial_n g = -1/L \,, \qquad \boldsymbol{x} \in \partial\Omega \,. \tag{3.41b}$$

Here L is the perimeter of ∂D. To satisfy the condition (3.11c), we chose the constant c in (3.39) as

$$c \int_\Omega \mu \, d\boldsymbol{x} = - \int_\Omega \mu \left(g_p + g \right) \, d\boldsymbol{x} \,. \tag{3.42}$$

In terms of this decomposition, the function R in (3.13) is given by

$$R(\boldsymbol{x}; \boldsymbol{x_0}) = g_p(\boldsymbol{x}) + \left(g(\boldsymbol{x}; \boldsymbol{x_0}) + \frac{1}{2\pi} \log |\boldsymbol{x} - \boldsymbol{x_0}| \right) + c(\boldsymbol{x_0}) \,. \tag{3.43}$$

As an example, consider a circular domain of radius one with $\mu = \mu(|\boldsymbol{x}|)$. For this case, where $L = 2\pi$, we identify points in the circle as complex numbers and then calculate g explicitly from (3.41) as

$$g(\boldsymbol{x}; \boldsymbol{x_0}) = -\frac{1}{2\pi} \log |\boldsymbol{x} - \boldsymbol{x_0}| - \frac{1}{2\pi} \log |\boldsymbol{x_0}| - \frac{1}{2\pi} \log |\boldsymbol{x} - 1/\bar{\boldsymbol{x}}_{\boldsymbol{0}}| \,. \tag{3.44}$$

Here $\bar{\boldsymbol{x}}_{\boldsymbol{0}}$ denotes the complex congugate of $\boldsymbol{x_0}$. From (3.40) we determine g_p as

$$g_p = \frac{1}{2\pi \mu_a} \int_0^r \frac{1}{s} \left(\int_0^s \eta \mu(\eta) \, d\eta \right) \, ds \,, \qquad \mu_a \equiv \int_0^1 r \mu(r) \, dr \,. \tag{3.45}$$

Substituting (3.44) and (3.45) into (3.43) we can calculate the gradient of R at $\boldsymbol{x_0}$ as

$$\boldsymbol{\nabla} R_0 \equiv \boldsymbol{\nabla} R(\boldsymbol{x}; \boldsymbol{x_0})|_{\boldsymbol{x}=\boldsymbol{x_0}} = \frac{1}{2\pi} \left[\frac{1}{1 - |\boldsymbol{x_0}|^2} + \frac{1}{\mu_a |\boldsymbol{x_0}|^2} \int_0^{|\boldsymbol{x_0}|} s \mu(s) \, ds \right] \boldsymbol{x_0} \,. \tag{3.46}$$

Substituting (3.46) into (3.37), and using (3.38), we obtain the following result.

Corollary 3.1: *Under the conditions of Proposition 3.2, let $\mu = \mu(|\boldsymbol{x}|)$ and suppose that Ω is a circular domain of radius one. Then, the motion of the center of the spike satisfies*

$$\frac{d\boldsymbol{x_0}}{dt} \sim -\varepsilon^2 \kappa \mu_a \left[\frac{1}{1 - |\boldsymbol{x_0}|^2} + \frac{1}{\mu_a |\boldsymbol{x_0}|^2} \int_0^{|\boldsymbol{x_0}|} s \mu(s) \, ds \right] \boldsymbol{x_0} \,, \tag{3.47a}$$

where μ_a is defined in (3.45) and

$$\kappa \equiv \frac{2q}{D(p-1)} \,. \tag{3.47b}$$

From (3.47), it follows that the spike will tend to the origin as $t \to \infty$. A differential equation for the distance from the center of the spike to the origin can be obtained by taking the dot product of (3.47a) with $\boldsymbol{x_0}$. As an example, suppose that $\mu \equiv 1$. Then, upon defining $\xi = \xi(t)$ by $\xi = |\boldsymbol{x_0}|^2$, we obtain from (3.47a) that

$$\frac{d\xi}{dt} \sim -\varepsilon^2 \kappa \left(\frac{2-\xi}{1-\xi} \right) \xi \,. \tag{3.48}$$

Upon integrating this differential equation we obtain the next result.
<u>**Corollary 3.2**</u>: *Let $\mu = 1$, $V \equiv 0$ and Ω be the unit circle. Suppose that the spike is initially centered at $\boldsymbol{x_0}(0) \in \Omega$. Then, when $\varepsilon \ll 1$ and $D \gg 1$, the distance from the spike to the origin at later times is given by*

$$|\boldsymbol{x_0}(t)| \sim \left(1 - \left[1 - \beta e^{-2\varepsilon^2 \kappa t} \right]^{1/2} \right)^{1/2} \,, \qquad \text{where} \qquad \beta \equiv 1 - \left(1 - |\boldsymbol{x_0}(0)|^2 \right)^2 \,. \tag{3.49}$$

Here κ is defined in (3.47b).

4 Finite Element Discretization

In this section we outline the numerical method used to compute solutions to (1.3). For simplicity, we write (1.3) in the following compact form

$$M \mathbf{u}_t = \nabla \cdot (K \nabla \mathbf{u}) + \mathbf{f}(\mathbf{u}, \boldsymbol{x}) \,, \tag{4.1a}$$

where $\mathbf{u} = (u, v)$ and

$$M \equiv \begin{pmatrix} 1 & 0 \\ 0 & 0 \end{pmatrix}, \qquad K \equiv \begin{pmatrix} \epsilon^2 & 0 \\ 0 & D \end{pmatrix} \quad \text{and} \quad \mathbf{f}(\mathbf{u}, \boldsymbol{x}) \equiv \begin{pmatrix} -[1+V(\boldsymbol{x})]u + u^p/v^q \\ -\mu v + \epsilon^{-2} u^r / v^s \end{pmatrix} . \tag{4.1b}$$

Before we define the finite element discretization of (4.1a), let us first introduce some notation. Let $0 = t_0 < t_1 < \ldots < t_N = T$ be a subdivision of $[0, T]$ with corresponding time steps $k_n = t_n - t_{n-1}$. For each n, $0 \le n \le N$, let $\mathcal{T}_n = \{\kappa\}$ be a finite element partition of Ω into shape regular simplices κ. For $p \in \mathbb{N}$ we define the finite element space

$$S_{h_n} = \{ w \in C(\Omega) : \; w|_\kappa \in \mathcal{P}_p(\kappa) \,, \; \forall \kappa \in \mathcal{T}_n \} \,, \tag{4.2}$$

for $n = 1, \ldots, N$, where $\mathcal{P}_p(\kappa)$ denotes the space of polynomials of degree at most p over κ.

The construction of the finite element method involves writing the problem (4.1a) in the following weak form: find $\mathbf{u}(t)$ such that

$$\begin{aligned}(M\mathbf{u}_t(\cdot,t),\mathbf{w}) &= -(K\nabla\mathbf{u}(\cdot,t),\nabla\mathbf{w}) + (\mathbf{f}(\mathbf{u}(\cdot,t),\cdot),\mathbf{w})\ , \quad \forall \mathbf{w}\in\mathcal{V}\,, &(4.3a)\\ (\mathbf{u}(\cdot,0),\mathbf{w}) &= (\mathbf{u}_0,\mathbf{w})\ , \quad \forall\mathbf{w}\in\mathcal{V}\,. &(4.3b)\end{aligned}$$

Here $(\cdot,\cdot)$ denotes the $L_2(\Omega)$ inner product, $\mathcal{V} = \left(H^1(\Omega)\right)^2$ and $H^1(\Omega)$ denotes the usual Hilbertian Sobolev space. The time–discretization involves approximating the derivative $\mathbf{u}_t$ by a divided difference operator. The simplest appropriate discretization is the backward Euler method, giving for $n = 1, \ldots, N$:

$$\begin{aligned}\left(M\frac{\mathbf{u}(\cdot,t_n)-\mathbf{u}(\cdot,t_{n-1})}{k_n},\mathbf{w}\right) &= -(K\nabla\mathbf{u}(\cdot,t_n),\nabla\mathbf{w}) + (\mathbf{f}(\mathbf{u}(\cdot,t_n),\cdot),\mathbf{w})\ , \quad \forall\mathbf{w}\in\mathcal{V}\,, &(4.4a)\\ (\mathbf{u}(\cdot,0),\mathbf{w}) &= (\mathbf{u}_0,\mathbf{w})\ , \quad \forall\mathbf{w}\in\mathcal{V}\,. &(4.4b)\end{aligned}$$

If we now define $\mathbf{u}_h^n = (u_h^n, v_h^n)$ to be the Galerkin finite element approximation to $\mathbf{u}(\cdot,t_n)$ at time t_n, then applying the finite element method to (4.4) yields the following formulation. Find $\mathbf{u}_h^n \in (S_{h_n})^2$ for $1 \le n \le N$ such that

$$\begin{aligned}\left(M\frac{\mathbf{u}_h^n-\mathbf{u}_h^{n-1}}{k_n},\mathbf{w}\right) &= -(K\nabla\mathbf{u}_h^n,\nabla\mathbf{w}) + (\mathbf{f}(\mathbf{u}_h^n,\boldsymbol{x}_n),\mathbf{w})\ , \quad \forall\mathbf{w}\in(S_{h_n})^2\,, &(4.5a)\\ \left(\mathbf{u}_h^0,\mathbf{w}\right) &= (\mathbf{u}_0,\mathbf{w})\ , \quad \forall\mathbf{w}\in(S_{h_n})^2\,. &(4.5b)\end{aligned}$$

For computational simplicity the nonlinear reaction term $\mathbf{f}(\mathbf{u}_h^n,\boldsymbol{x}_n)$ on the right–hand side of (4.5a) is linearized about the finite element solution $\mathbf{u}_h^{n-1}$ at the previous time level t_{n-1}. The numerical method described above is similar to that given in [1] and [9].

5 Asymptotic and Numerical Results in One Dimension

For the special case where $(p,q,r,s) = (2,1,2,0)$ we compare the asymptotic results presented in §2 with corresponding numerical results. In each of the figures below, the solid curves are obtained from solving the full problem (1.1) numerically using the finite-element method described in §4 with approximately 1001 elements. The crosses in these figures represent the asymptotic results obtained from solving the relevant differential equation of §2 numerically using a standard solver routine from Maple [4].

5.1 Experiment 1

We take the parameter values $V(x) \equiv 0$, $\mu(x) = 1$, $D = 1$, and $\epsilon = 0.03$. The initial condition used for the finite element solution, as obtained from (2.3c), (2.15a) and (2.15b), is

$$a(x,0) = \frac{3H}{2}\operatorname{sech}^2\left(\frac{x-x_0}{2\epsilon}\right), \tag{5.1a}$$

$$h(x,0) = H\frac{G(x;x_0)}{G(x_0;x_0)}, \tag{5.1b}$$

where from (2.14b)

$$H = \left[6G(x_0;x_0)\right]^{-1} . \tag{5.1c}$$

In this case, the initial condition $a(x,0)$ consists of a spike in the activator concentration centered at $x_0 = 0.6$. The asymptotic result for the motion of the center of the spike obtained from (2.19) is

$$\frac{dx_0}{dt} \sim -(0.03)^2\left[\tanh(1+x_0) - \tanh(1-x_0)\right] , \tag{5.2}$$

with $x_0(0) = 0.6$. In Fig. 2 and Table 1 we show the favorable agreement between the asymptotic and numerical results for the motion of the center of the spike. For this example, the spike drifts towards the center of the interval.

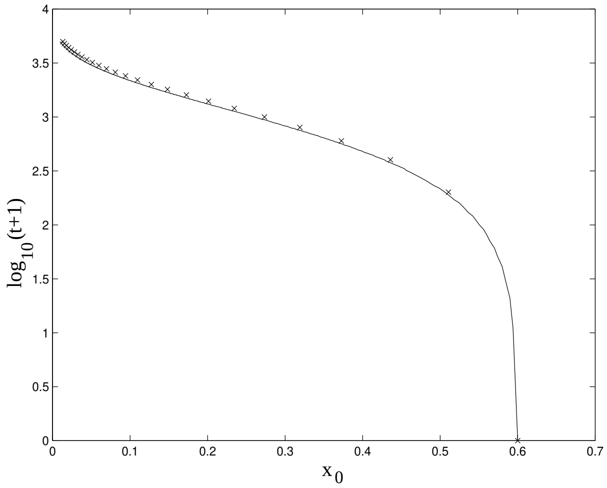

Figure 2: The trajectory $x_0(t)$ of the spike in the activator concentration. The solid curve is the numerical result and the crosses are obtained from solving the asymptotic result (5.2) numerically.

t	$\log_{10}(t+1)$	$x_0(t)$ (num)	$x_0(t)$ (asm)
0	0.0	0.6000	0.6
10	1.041	0.5940	0.5951
100	2.0043	0.5500	0.5534
200	2.3032	0.5060	0.5107
400	2.6031	0.4280	0.4358
800	2.9036	0.3060	0.3189
1600	3.2044	0.1600	0.1727
3200	3.5053	0.0440	0.0514

Table 1: The numerical and asymptotic results for $x_0(t)$ corresponding to a selection of the values plotted in Fig. 2.

5.2 Experiment 2

The parameter values here are $V(x) \equiv \frac{1}{2}(x-\frac{1}{4})^2$, $\mu(x)=1$, $D=1$, and $\epsilon=0.03$. The initial condition used for the finite element solution is

$$a(x,0) = \frac{3}{2}H\left(1+V[x_0]\right)\operatorname{sech}^2\left(\frac{\sqrt{1+V[x_0]}(x-x_0)}{2\epsilon}\right), \tag{5.3a}$$

$$h(x,0) = H\frac{G(x;x_0)}{G(x_0;x_0)}, \tag{5.3b}$$

where

$$H = \left[6G(x_0;x_0)\right]^{-1}\left[1+V(x_0)\right]^{-3/2}. \tag{5.3c}$$

As in the previous experiment, we choose the initial spike location to be at $x_0(0)=0.6$. In this case, the differential equation for the spike location $x_0(t)$, as obtained from (2.19), is

$$\frac{dx_0}{dt} \sim -(0.03)^2\left(\tanh(1+x_0)-\tanh(1-x_0)+\frac{5(x_0-\frac{1}{4})}{2+(x_0-\frac{1}{4})^2}\right), \tag{5.4}$$

with $x_0(0)=0.6$. As a result of the competition between the hyperbolic tangent functions and the precursor gradient $V(x)$, the spike does not approach the center of the interval as $t\to\infty$. Instead, by setting the right-hand side of (5.4) to zero, it follows that (5.4) has a unique stable equilibrium location $x_0^e \neq 0$ for which $\lim_{t\to\infty} x_0(t) \to x_0^e \approx 0.184$. In Fig. 3 and Table 2 we favorably compare the asymptotic and numerical results for the motion of the center of the spike.

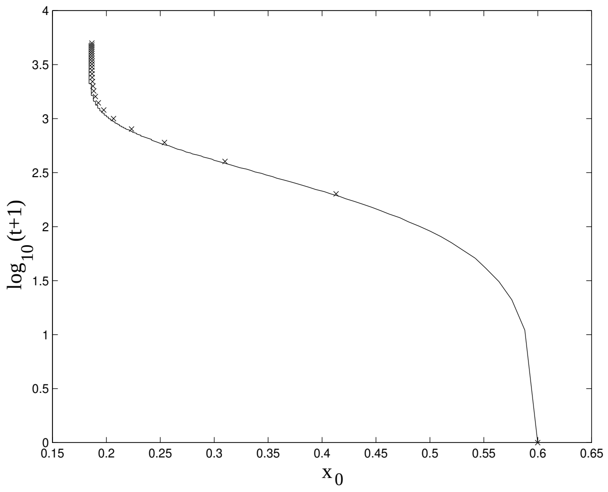

Figure 3: The trajectory $x_0(t)$ of the spike in the activator concentration. The solid curve is the numerical result and the crosses are obtained from solving the asymptotic result (5.4) numerically.

5.3 Experiment 3

The parameter values are $V(x) \equiv \frac{1}{2}(x - \frac{1}{4})^2$, $\mu(x) = 1$, $D = 50$, and $\epsilon = 0.03$. The initial conditions are as in the previous experiment. In this case the appropriate differential equation is (2.24), which reduces to

$$\frac{dx_0}{dt} \sim -(0.03)^2 \left(\frac{x_0}{25} + \frac{5(x_0 - \frac{1}{4})}{2 + (x_0 - \frac{1}{4})^2} \right), \tag{5.5}$$

with $x_0(0) = 0.6$. From this differential equation it follows that the equilibrium position of the spike is approximately $\frac{1}{4}$, since the contribution to the dynamics from the first term is negligible. Thus, in this case the spike tends to the minimum value of the potential function $V(x)$ as $t \to \infty$. The asymptotic and numerical results for the center of the spike as a function of time are compared in Fig. 4 and Table 3.

5.4 Experiment 4

Here we set $V(x) \equiv 0$, $\mu(x) = 2e^{-(x+1)}$, $D = 50$ and $\epsilon = 0.03$. We take the same initial conditions as in experiment 1. For this example, the spike location satisfies (2.24), which reduces to

$$\frac{dx_0}{dt} \sim -\frac{(0.03)^2}{25} \left(2 \int_{-1}^{x_0} e^{-(x+1)} \mathrm{d}x - \mu_a \right), \tag{5.6}$$

t	$\log_{10}(t+1)$	$x_0(t)$ (num)	$x_0(t)$ (asm)
0	0.0	0.6000	0.6
10	1.041	0.5880	0.5879
100	2.0043	0.4900	0.4929
200	2.3032	0.4080	0.4130
400	2.6031	0.3040	0.3100
800	2.9036	0.2180	0.2234
1600	3.2044	0.1880	0.1899
3200	3.5053	0.1840	0.1867

Table 2: The numerical and asymptotic results for $x_0(t)$ corresponding to a selection of the values plotted in Fig. 3.

t	$\log_{10}(t+1)$	$x_0(t)$ (num)	$x_0(t)$ (asm)
0	0.0	0.6000	0.6
10	1.041	0.5920	0.5924
100	2.0043	0.5320	0.5306
200	2.3032	0.4740	0.4740
400	2.6031	0.3920	0.3914
800	2.9036	0.3060	0.3045
1600	3.2044	0.2560	0.2555
3200	3.5053	0.2460	0.2463

Table 3: The numerical and asymptotic results for $x_0(t)$ corresponding to a selection of the values plotted in Fig. 4.

with $x_0(0) = 0.6$. From (5.6) it follows that there is a unique stable equilibrium value x_0^e satisfying

$$\int_{-1}^{x_0^e} \mu(y)\mathrm{d}y = \mu_a, \qquad \text{where} \qquad \mu_a = \frac{1}{2}\int_{-1}^{1} \mu(y)\mathrm{d}y\,. \tag{5.7}$$

Using $\mu(x) = 2e^{-(x+1)}$, (5.7) yields $x_0^e = -1 - \log(1 - \frac{\mu_a}{2}) \approx -0.434$ and thus $\lim_{t\to\infty} x_0(t) \to x_0^e$. Asymptotic and numerical results for the center of the spike as a function of time are compared in Fig. 5 and Table 4.

5.5 Experiment 5

Here we take $V(x) \equiv \frac{1}{2}(x - \frac{1}{4})^2$, $\mu(x) = 2e^{-(x+1)}$, $D = 1.0$ and $\epsilon = 0.03$. We take the same initial conditions as in experiment 2.

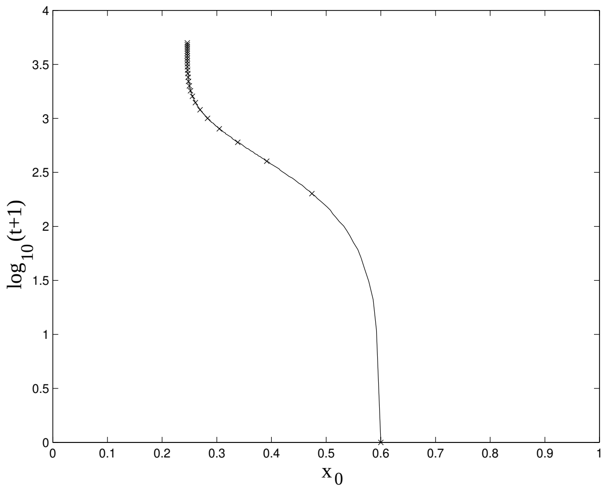

Figure 4: The trajectory $x_0(t)$ of the spike in the activator concentration. The solid curve is the numerical result and the crosses are obtained from solving the asymptotic result (5.5) numerically.

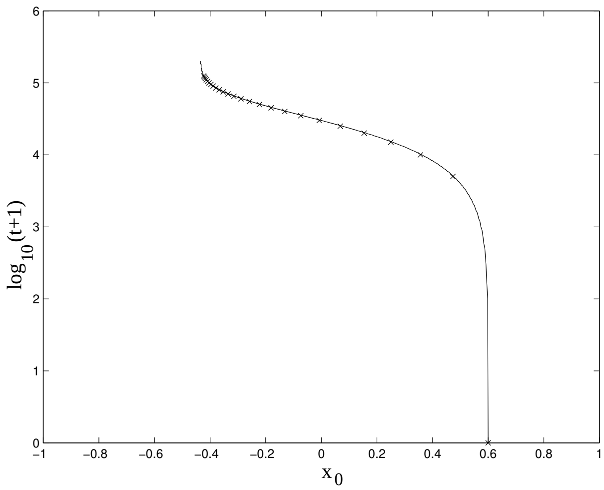

Figure 5: The trajectory $x_0(t)$ of the spike in the activator concentration. The solid curve is the numerical result and the crosses are obtained from solving the asymptotic result (5.6) numerically.

t	$\log_{10}(t+1)$	$x_0(t)$ (num)	$x_0(t)$ (asm)
0	0	0.6000	0.6
100	2.0043	0.5980	0.5974
200	2.3032	0.5940	0.5947
400	2.6031	0.5900	0.5895
800	2.9036	0.5800	0.5791
1600	3.2044	0.5600	0.5584
3200	3.5053	0.5200	0.5177
6400	3.8062	0.4420	0.4395
12800	4.1072	0.3020	0.2955
25600	4.4081	0.0660	0.0748
51200	4.7095	-0.2260	-0.2166
102400	5.0104	-0.4060	-0.4018

Table 4: The numerical and asymptotic results for $x_0(t)$ corresponding to a selection of the values plotted in Fig. 5.

For this example, the spike location satisfies the differential equation (2.17). In order to evaluate the Green's function appearing in the asymptotic result (2.17), we solved the boundary value problem (2.12) numerically using COLSYS [2] for a range of x_0 values. A spline interpolant was then used to evaluate the first term on the right-hand side of (2.17) at an arbitrary value of x_0. The stable equilibrium value for (2.17) was found numerically to be $x_0^e \approx 0.056$. Thus, we have that $\lim_{t\to\infty} x_0(t) \to 0.056$. Asymptotic and numerical results for the center of the spike as a function of time are compared in Fig. 6 and Table 5.

5.6 Experiment 6

In this experiment we study the case where the initial condition in the activator concentration a consists of two spikes centered near their equilibrium values at $x = 0.5$ and $x = -0.5$. The parameter values are taken to be $V(x) \equiv 0$, $\mu(x) = 1$ and $\epsilon = 0.03$.

We first choose $D = 0.370$. In this case both spikes tend to their equilibrium positions as shown in Fig. 7a. Alternatively, if we take $D = 0.375$ one of the spikes is eventually annihilated and the remaining spike tends to the midpoint of the interval as shown in Fig. 7b. Thus, the criterion for whether an initial two-spike solution will remain a two-spike solution for all time depends both on D and on the initial location of the spikes.

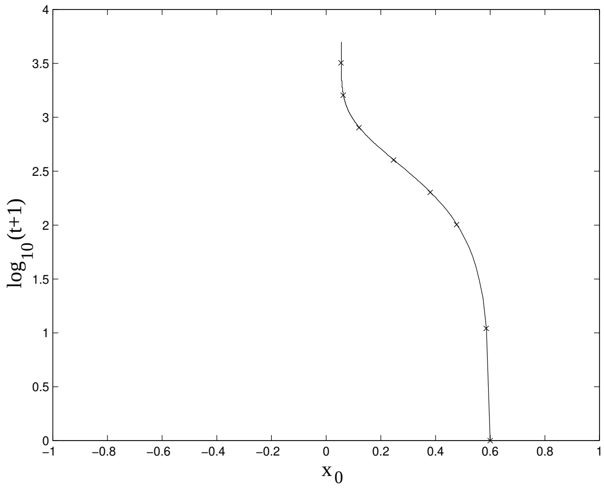

Figure 6: The trajectory $x_0(t)$ of the spike in the activator concentration. The solid curve is the numerical result and the crosses are obtained from solving the asymptotic result (2.17) numerically.

t	$\log_{10}(t+1)$	$x_0(t)$ (num)	$x_0(t)$ (asm)
0	0.0	0.6000	0.6
10	1.041	0.5860	0.5854
100	2.0043	0.4780	0.4771
200	2.3032	0.3820	0.3808
400	2.6031	0.2480	0.2464
800	2.9036	0.1220	0.1200
1600	3.2044	0.0640	0.0621
3200	3.5053	0.0560	0.0557

Table 5: The numerical and asymptotic results for $x_0(t)$ corresponding to the values plotted in Fig. 6.

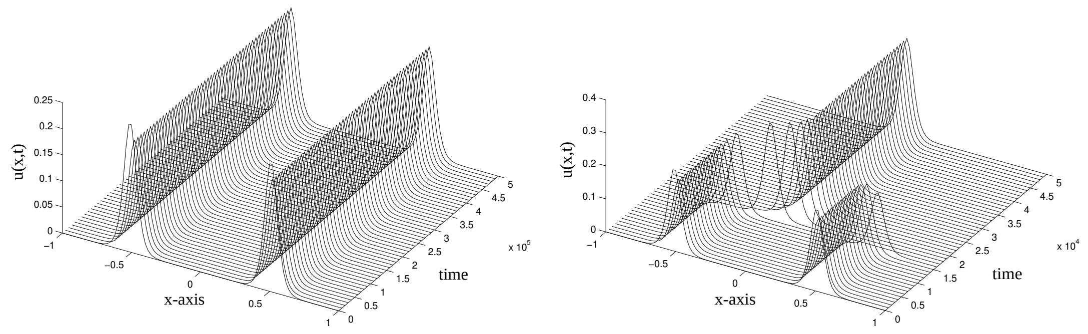

(a) $a(x,t)$ for $D = 0.370$

(b) $a(x,t)$ for $D = 0.375$

Figure 7: Numerical solution of activator $u(x,t)$ with parameters $\epsilon = 0.03,\ \mu = 1.0$.

5.7 Experiment 7

In this experiment we study the case where the initial condition in the activator concentration a consists of two spikes centered far from their equilibrium values at $x = 0.5$ and $x = -0.5$. The parameter values are taken to be $V(x) \equiv 0$, $\mu(x) = 1$ and $\epsilon = 0.03$. The value of D at which the solution tends to a stable two-spike equilibrium solution in the previous experiment Fig. 7a now leads to a solution in which only one spike is stable (see Fig. 8b). On choosing $D = 0.25$ both spikes now tend to their equilibrium values as shown in Fig. 8a.

6 Asymptotic and Numerical Results in Two Dimensions

For the special case where $(p,q,r,s) = (2,1,2,0)$ we compare the asymptotic results presented in §3 with corresponding numerical results. For each of the examples below we take a circular domain of radius one. In the numerical computations shown, we took 8321 nodes and 16384 elements for the finite element method of §4. The circular domain was triangulated in a manner similar to that shown in Fig. 9. A fixed time step, $\Delta t = 0.1$ was chosen in the simulations. The general form of the initial conditions used in the simulations is

$$a(\boldsymbol{x},0) = \sum_{i=1}^{m} \operatorname{sech}^8 \left[|\boldsymbol{x} - \boldsymbol{x_i}| \right] , \tag{6.1a}$$

$$h(\boldsymbol{x},0) = 100.0 \, , \tag{6.1b}$$

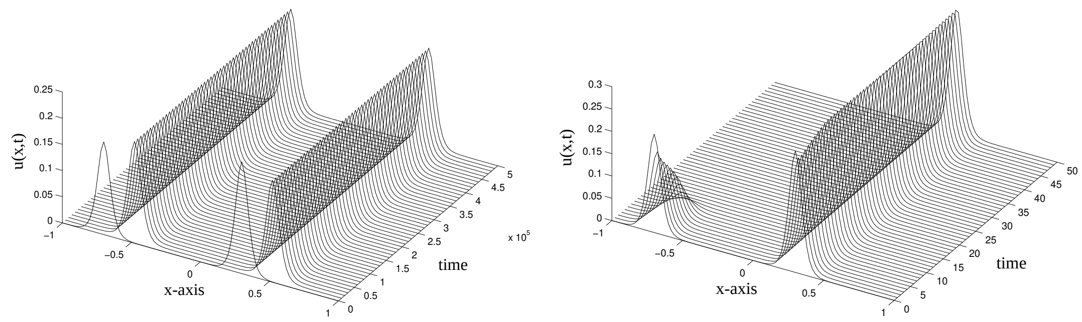

(a) $a(x,t)$ for $D = 0.25$ (b) $a(x,t)$ for $D = 0.370$

Figure 8: Numerical solution of activator $u(x,t)$ with parameters $\epsilon = 0.03,\ \mu = 1.0$.

where $\boldsymbol{x_i}$ is the location of the i^{th} spike and m is the number of spikes.

6.1 Experiment 1: The Effect of D when $V \equiv 0$

We set $V(x) \equiv 0$ and $\mu(x) = 1$. The initial condition for a in (6.1) is taken to consist of a single spike in the activator concentration centered at $(-0.5, -0.5)$. The asymptotic result for the distance of the spike to the origin is given in (3.49) and it is valid when $\varepsilon \ll 1$ and $D \gg 1$. In Fig. 10a, where $D = 10$ and $\varepsilon = 0.06$, we show the close agreement between the full numerical result for the distance of the spike to the origin and the asymptotic result obtained from (3.49). The asymptotic result (3.49) is no longer valid when $D = O(1)$ since the leading order problem (3.30) is coupled. In Fig. 10b, where $D = 1$ and $\varepsilon = 0.03$, we show the rather poor agreement between the full numerical result for the distance of the spike to the origin and the result obtained from (3.49). It would be interesting to analytically characterize the one-spike dynamics when $D = O(1)$. However, we expect that this is a difficult problem. We remark that a limitation of the numerical method used to generate Fig. 10a and Fig. 10b is that they were done with a small fixed time step. To improve accuracy and minimize computational costs over a long time interval, it would be preferable to implement a variable time-step strategy with error control.

6.2 Experiment 2: The Effect of the Potential V

We take $V(\boldsymbol{x}) \equiv \frac{1}{4}|\boldsymbol{x} - \xi|^2$ where $\xi = (0.25, -0.25)$, so that the potential W in (3.26) has a minimum at $\boldsymbol{x} = \xi$. From (3.26) we expect that $\boldsymbol{x} \to \xi$ as $t \to \infty$. The other parameter values are $D = 25$,

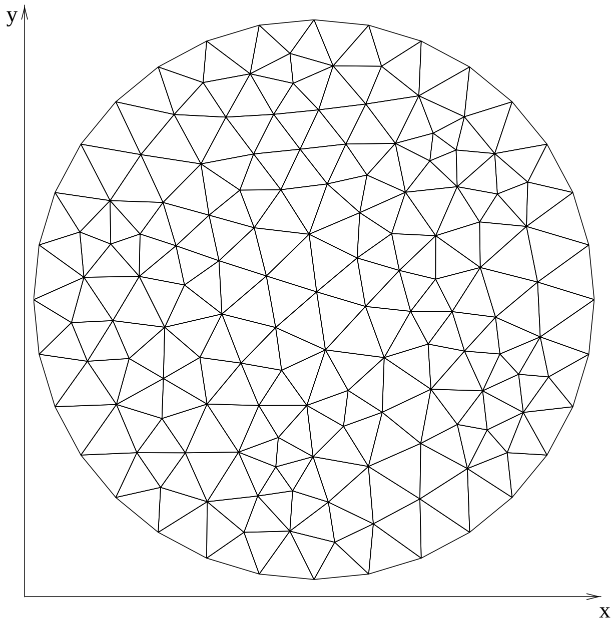

Figure 9: A regular triangulation of a circular domain.

$\mu = 1$ and $\varepsilon = 0.10$. Since $D \gg 1$, the asymptotic result for the spike motion is (3.26). The initial condition in a, given in (6.1a), is taken to be a single spike centered at $\mathbf{x_0}(0) = (-0.5, -0.5)$. From the asymptotic result (3.26), we can derive the following system for the coordinates $\boldsymbol{x_0} = (x_0, y_0)$ of the center of the spike:

$$\frac{dx_0}{dt} \sim -\frac{4\varepsilon^2(x_0 - \xi_1)}{4 + |\boldsymbol{x_0} - \xi|}, \qquad \frac{dy_0}{dt} \sim -\frac{4\varepsilon^2(y_0 - \xi_2)}{4 + |\boldsymbol{x_0} - \xi|}. \tag{6.2}$$

Here $\xi = (\xi_1, \xi_2)$. In Fig. 11a we show the close agreement between the full numerical result for the distance of the spike to the origin and the corresponding asymptotic result obtained from integrating (6.2) numerically using Maple [4]. In Fig. 11b we show that the trajectory of the spike is approximately orthogonal to the level curves of the potential W as predicted by (3.26).

6.3 Experiment 3: Several Initial Spikes

In this experiment we examine numerically the behavior of the solution to (1.3) at two different values of D when the initial condition in a consists of two spikes centered at $(-0.5, 0.0)$ and $(0.5, 0.0)$. The parameter values are $V(x) \equiv 0$, $\mu(x) = 1$, and $\varepsilon = 0.03$. This experiment is similar to experiment 8 for the corresponding one-dimensional problem where two initial spikes are centered at arbitrary locations.

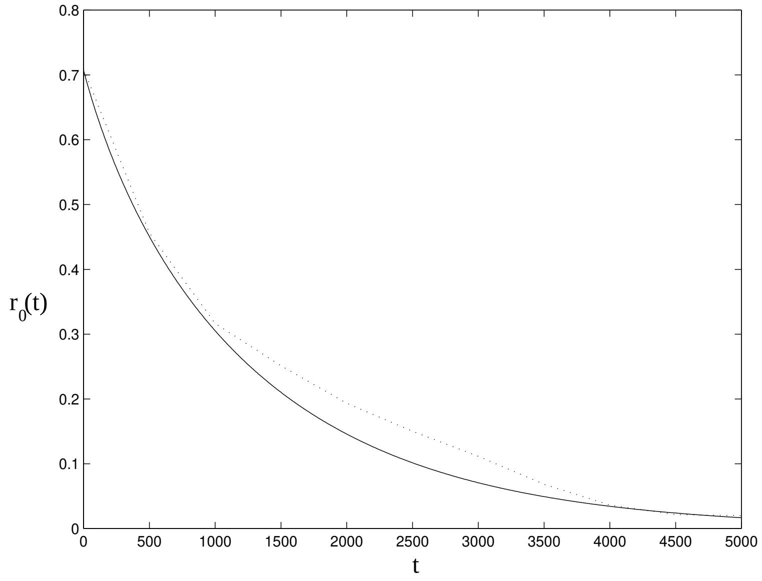

Figure 10a: The distance from the center of the spike to the origin for experiment 1 when $D = 10$ and $\varepsilon = 0.06$. The dotted curve is the full numerical result and the solid curve is the asymptotic result (3.49).

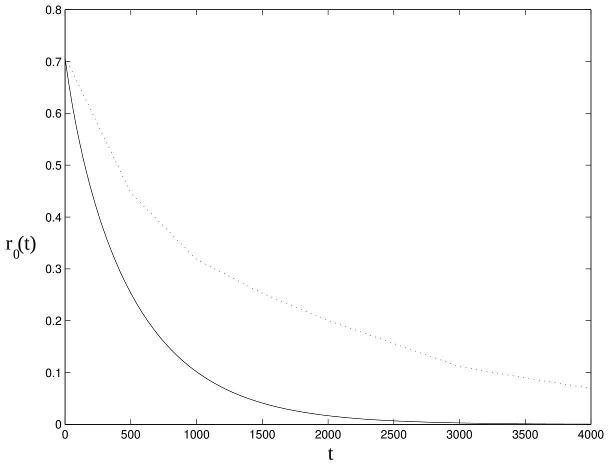

Figure 10b: The distance from the center of the spike to the origin for experiment 1 when $D = 1$ and $\varepsilon = 0.03$. The dotted curve is the full numerical result and the solid curve is the asymptotic result (3.49).

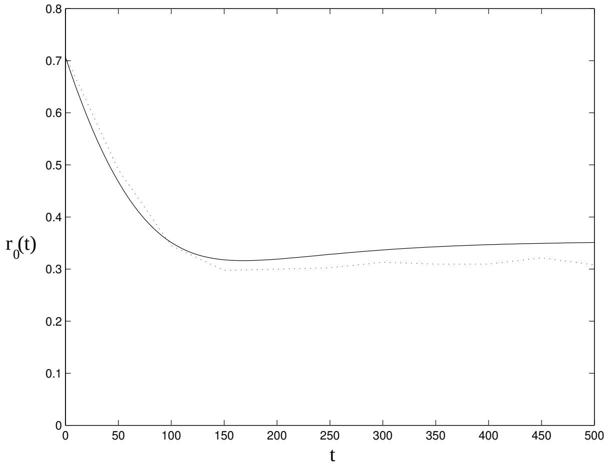

Figure 11a: The distance from the center of the spike to the origin for experiment2. The dotted curve is the full numerical result and the solid curve is the asymptotic result (6.2).

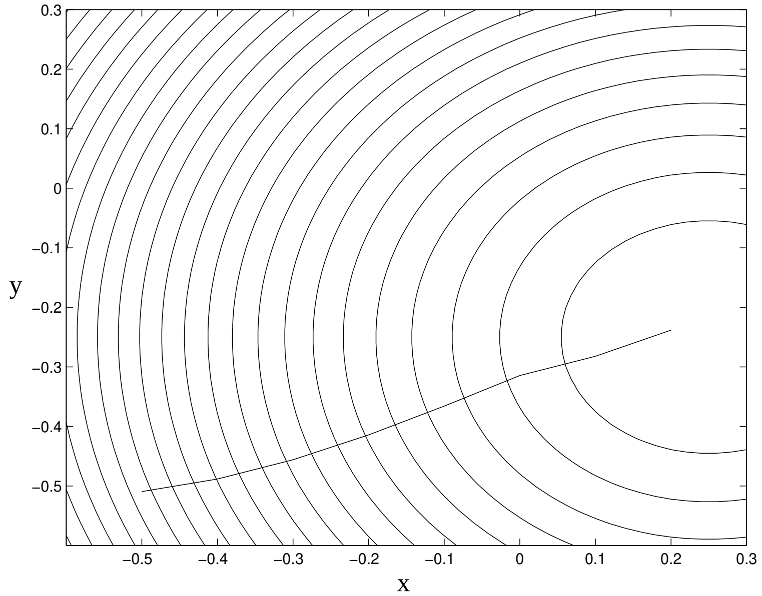

Figure 11b: The dotted line is the spike trajectory from the full numerical result for experiment 2 and the solid lines are the level curves of the potential W as defined in (3.26).

We first take $D = 0.5$. For this value of D, both of the spikes tend to certain equilibrium locations on the circle as shown in Fig. 12a and Fig. 12b.

Next, we take $D = 1.0$. The computational results at various times are shown in Fig. 13a–13d. For this value of D, we observe that one of the spikes is annihilated rather quickly while the remaining spike drifts very slowly towards the center of the circle.

This experiment only broaches the difficult topic of the stability and dynamics of multi-spike solutions in multi-dimensional domains. A goal of future work is to give a complete characterization of the dynamics and stability of such solutions.

Acknowledgements

M. J. W. is grateful for the support of NSERC grant 81541 and the hospitality of Hilary and John Ockendon of OCIAM at Oxford University where this paper was initiated. D. M. has been supported by a Marie Curie Fellowship as part of the Training and Mobility of Researchers (TMR) program administered by the European Commission.

A Calculating Some Integrals in §2

Here we show how to calculate the integrals appearing in (2.15c). We define them as

$$e \equiv \frac{\int_{-\infty}^{\infty} \left[u_c(y)\right]^2 \, dy}{\int_{-\infty}^{\infty} \left[u_c'(y)\right]^2 \, dy}, \qquad f \equiv \frac{\int_{-\infty}^{\infty} \left[u_c(y)\right]^{p+1} \, dy}{\int_{-\infty}^{\infty} \left[u_c'(y)\right]^2 \, dy}. \tag{A.1}$$

We first multiply (2.3a) by u_c. Upon integrating the resulting equation over the domain we obtain

$$\int_{-\infty}^{\infty} u_c u_c'' \, dy - [1 + V(x_0)] \int_{-\infty}^{\infty} u_c^2 \, dy + \int_{-\infty}^{\infty} u_c^{p+1} \, dy = 0\,. \tag{A.2}$$

Upon integrating the first term in this equation by parts we get

$$-1 = [1 + V(x_0)]\, e - f\,. \tag{A.3}$$

To obtain an additional equation we multiply (2.3a) by u_c' and integrate over the domain to fix the constant of integration. We then integrate the resulting expression again to get

$$1 = [1 + V(x_0)]\, e - \frac{2f}{p+1}\,. \tag{A.4}$$

Solving (A.3) and (A.4) we get the key results

$$f = \frac{2(p+1)}{p-1}, \qquad e = \frac{1}{1 + V(x_0)} \left(\frac{p+3}{p-1} \right). \tag{A.5}$$

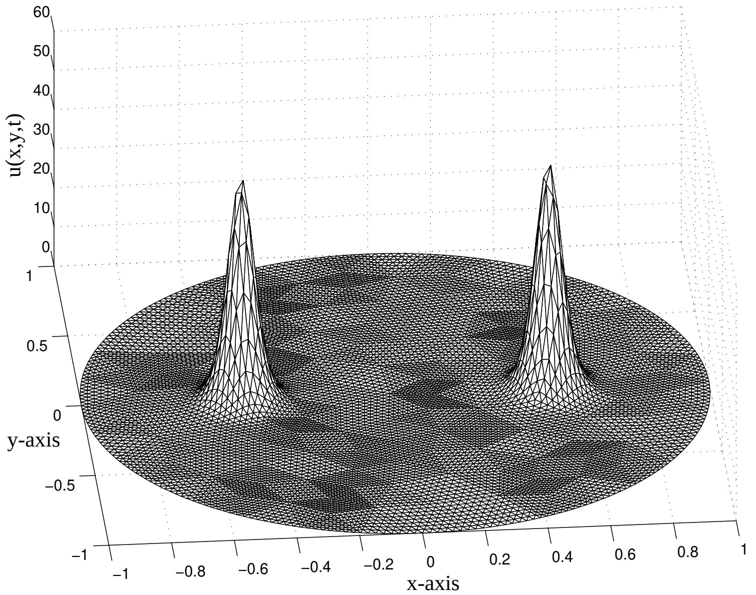

Figure 12a: The numerical solution of $a(\boldsymbol{x}, t)$ at t = 100.0 with parameters $\epsilon = 0.03$, $\mu = 1.0$ and $D = 0.5$.

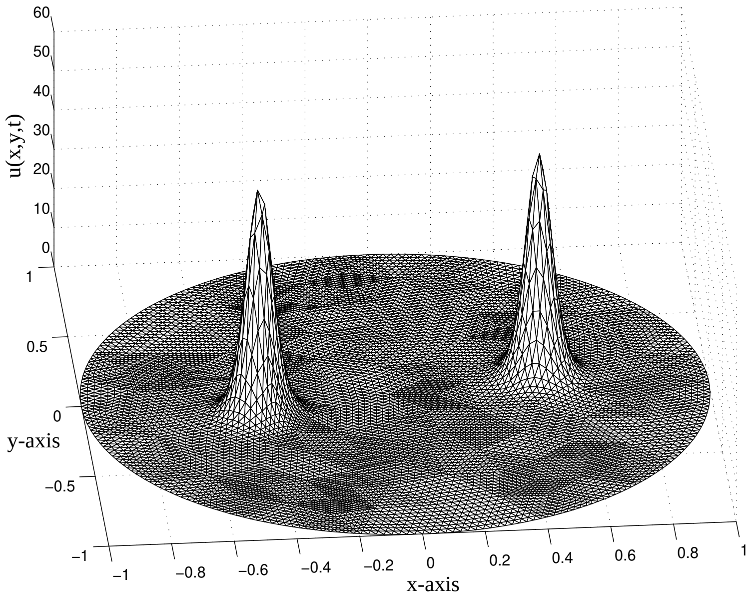

Figure 12b: The numerical solution of $a(\boldsymbol{x}, t)$ at t = 3000.0 with parameters $\epsilon = 0.03$, $\mu = 1.0$ and $D = 0.5$.

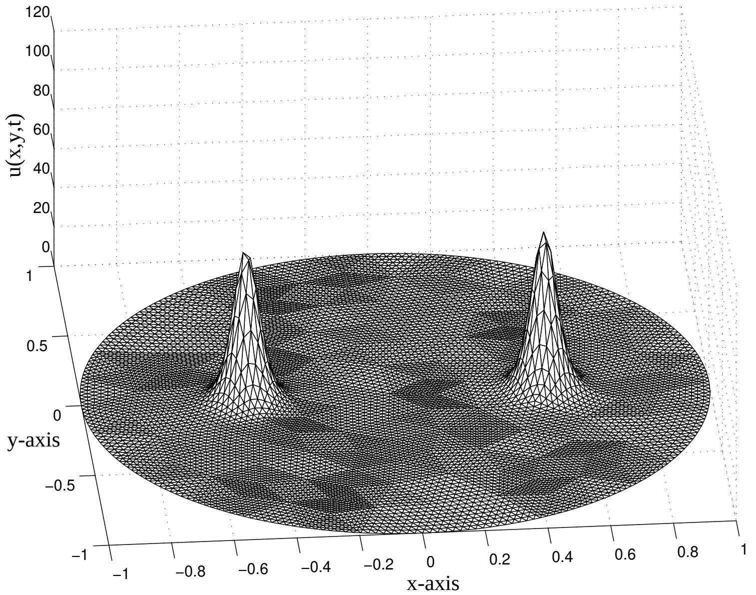

Figure 13a: The numerical solution of $a(\boldsymbol{x}, t)$ at t = 10.0 with parameters $\epsilon = 0.03$, $\mu = 1.0$ and $D = 1.0$.

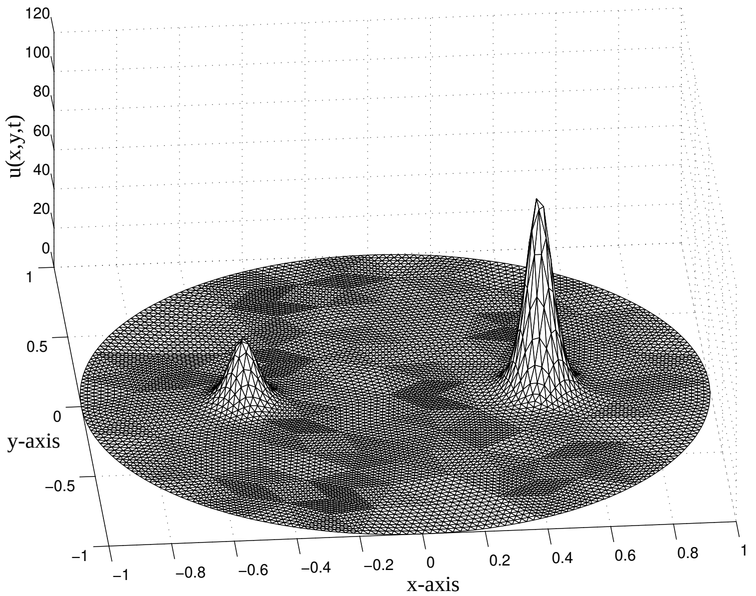

Figure 13b: The numerical solution of $a(\boldsymbol{x}, t)$ at t = 160.0 with parameters $\epsilon = 0.03$, $\mu = 1.0$ and $D = 1.0$.

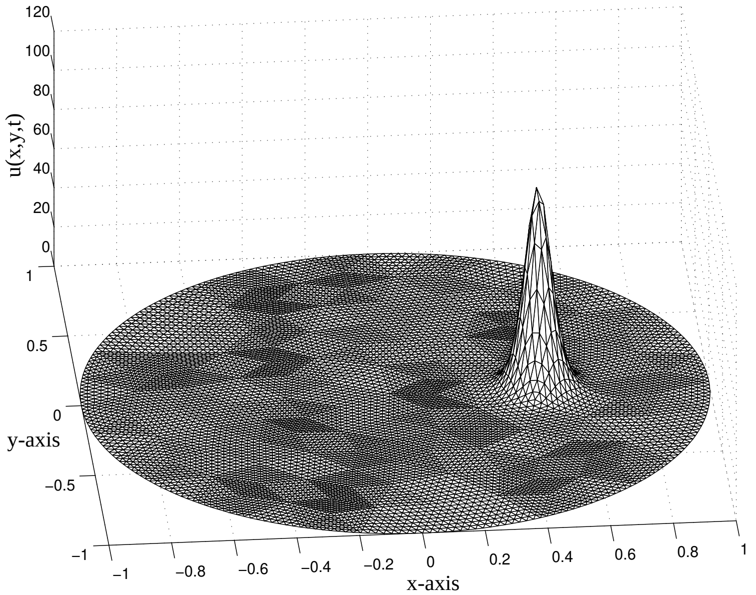

Figure 13c: The numerical solution of $a(\boldsymbol{x}, t)$ at t = 170.0 with parameters $\epsilon = 0.03$, $\mu = 1.0$ and $D = 1.0$.

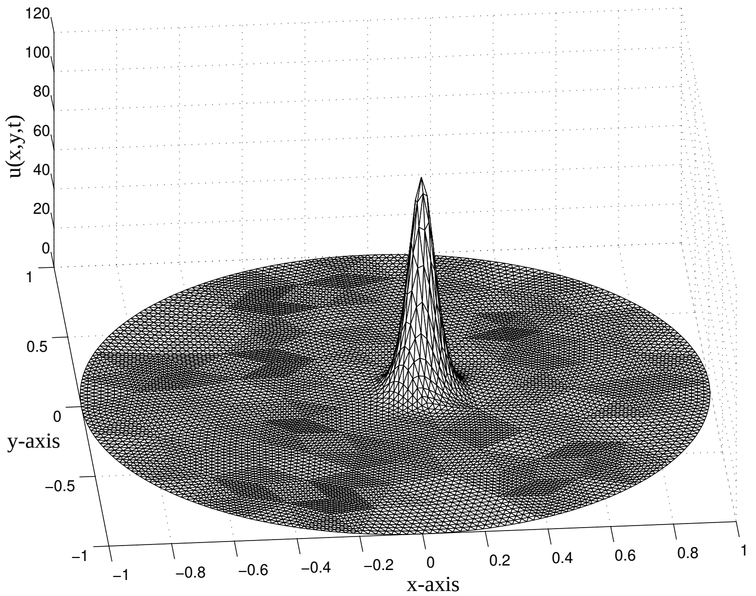

Figure 13d: The numerical solution of $a(\boldsymbol{x}, t)$ at t = 3000.0 with parameters $\epsilon = 0.03$, $\mu = 1.0$ and $D = 1.0$.

B Calculating Some Integrals in §3

We define the integrals in (3.25) and (3.38) by b and f respectively. They are given by

$$b \equiv \frac{\int_0^\infty [w_c(\eta)]^2 \, \eta \, d\eta}{\int_0^\infty [w_c'(\eta)]^2 \, \eta \, d\eta}, \qquad f \equiv \frac{\int_0^\infty [w_c(\eta)]^{p+1} \, \eta \, d\eta}{\int_0^\infty [w_c'(\eta)]^2 \, \eta \, d\eta}. \tag{B.1}$$

We show how to calculate them in terms of the solution w_c to (3.24).

We first multiply (3.24a) by ηw_c. Upon integrating the resulting equation over the domain we obtain

$$\int_0^\infty w_c \left(\eta w_c'\right)' \, d\eta - \int_0^\infty \eta w_c^2 \, d\eta + \int_0^\infty \eta w_c^{p+1} \, d\eta = 0. \tag{B.2}$$

Upon integrating the first term in this equation by parts, we get

$$f = b + 1. \tag{B.3}$$

To obtain an additional equation we multiply (3.24a) by $\eta^2 w_c'$ and integrate over the domain. Upon integrating by parts, and using the decay of w_c at infinity, we obtain

$$b = 2f/(p+1). \tag{B.4}$$

Solving (B.3) and (B.4) we get the key results

$$f = \frac{p+1}{p-1}, \qquad b = \frac{2}{p-1}. \tag{B.5}$$

References

[1] G. Akrivis, M. Crouzeix, C. Makridakis, *Implicit-Explicit Multistep Finite Element Methods for Nonlinear Parabolic Problems*, Math. Comp. **67**, (1998), pp. 457-477.

[2] U. Ascher, R. Christiansen, R. Russell, *Collocation Software for Boundary Value ODE's*, Math. Comp. **33**, (1979), pp. 659-679.

[3] S.J. Chapman, G. Richardson, *Vortex Pinning by Inhomogeneities in Type-2 Superconductors*, Physica D, **108**, (1997), pp. 397-407.

[4] B. W. Char et al. *Maple 5 Reference Manual*, Springer-Verlag, (1991).

[5] X. Chen, M. Kowalcyzk, *Dynamics of an Interior Spike in the Gierer-Meinhardt System*, submitted, SIAM. J. Math. Anal., (1999).

[6] A. Gierer, H. Meinhardt, *A Theory of Biological Pattern Formation*, Kybernetik, **12**, (1972), pp. 30–39.

[7] L. Harrison, D. Holloway, *Order and Localization in Reaction-Diffusion Pattern*, Physica A, **222**, (1995), pp. 210-233.

[8] D. Iron, M. J. Ward, *A Metastable Spike Solution for a Non-Local Reaction-Diffusion Model*, SIAM J. Appl. Math., (2000), to appear.

[9] S. Larsson, *Numerical Analysis of Semilinear Parabolic Problems*, in *The Graduate Student's Guide to Numerical Analysis '98*: M. Ainsworth, J. Levesley and M. Marletta (editors), Lecture Notes from the VIII EPSRC Summer School in Numerical Analysis. Springer Verlag, 1999.

[10] F. H. Lin, Q. Du, *Ginzburg-Landau Vortices: Dynamics, Pinning and Hysteresis*, SIAM J. Math. Anal., **28**, (1997), pp. 1265-1293.

[11] P. K. Maini, K. J. Painter, H. N. P. Chau, *Spatial pattern formation in chemical and biological systems,* Faraday Transactions, **93**, (1997), pp. 3601-3610.

[12] H. Meinhardt, *Models of Biological Pattern Formation*, Academic Press, London (1982).

[13] NAG Fortran library Mark 17, routine D03PCF, Numerical Algorithms Group Ltd. Oxford, United Kingdom (1995).

[14] W. Ni, *Diffusion, Cross-Diffusion, and their Spike-Layer Steady-States*, Notices of the AMS, Vol. **45**, No. 1, (1998), pp. 9-18.

[15] A. Turing, *The Chemical Basis of Morphogenesis.* Phil. Trans Roy. Soc. B **237**, (1952), pp. 37-72.